NTNU
Det skapende universitet

Elastic to Non-Elastic Rock Deformation Studied by Combination of Static and Dynamic Measurements

Investigating the Behaviour of the
Non-Elastic Response

Tore Lie Sirevaag

Petroleumsfag
Innlevert: juni 2016
Hovedveileder: Andreas Bauer, IPT

Norges teknisk-naturvitenskapelige universitet
Institutt for petroleumsteknologi og anvendt geofysikk

Abstract

There is an underlying potential to use non-elastic rock properties for field and well applications. This knowledge might give additional information, in particular on cracks and fractures that cannot be obtained from linear elastic measurements. It turns out two effects are superposed during large alteration in stress and strain; the stress dependence of the rock stiffness and plasticity effects. Earlier quasi-static measurements on dry, clean free sandstone have investigated plasticity effects by unloading stress on a core sample. The results indicate that upon unloading from a turning point, the non-elastic compliance show a linear increase with stress alteration. Since compaction experiments are affected by artefacts when switching from loading to unloading or vice versa, the non-elastic compliance is used to obtain an extrapolated line to the beginning of the unloading path. The experiments in this thesis have been performed in a standard setup for triaxial rock mechanical measurements, with an integrated low frequency module, which allow for direct dynamic measurements. By modulating dynamic measurements, it is possible to look into the stress dependence of the stiffness, and investigate the dynamic non-elastic compliance. Comparison of the plot for dynamic and static non-elastic compliance show a strong correlation, and the dynamic measurements indicate that the extrapolated range also behaves linear. Since the low frequency measurements are obtained from strain gauges attached on the core sample, there was an opportunity to investigate the reliability of the taped strain gauges as well. Concerns from the scientific community about the method of taping strain gauges instead of gluing them, led to a decision to compare the taped against the glued. The comparison shows small difference in the experimental values, and the results show a similar trend behaviour when plotted.

Sammendrag

Det er et underliggende potensiale om å bruke ikke-lineære egenskaper til stein i brønn – og feltapplikasjoner. Denne kunnskapen kan muligens anvendes til å gi ny og nyttig informasjon om bestemte sprekker og forkastninger. Det viser seg at to effekter overlapper hverandre når man utsetter steinen for store spenninger; spenningsavhengighet for steinens stivhet og plastiske effekter. Tidligere studier gjort på ren sandstein har undersøkt den plastiske effekten ved reduksjon av spenning på en kjerneprøve. Ved reduksjon i spenning har man gjort observasjoner som viser en lineær oppførsel for den ikke-elastiske mykheten til steinen. Ved å anvende denne lineære oppførselen til steinen kan man ekstrapolere resultatområdet frem til begynnelsen av vendepunktet. Forsøkene i denne avhandlingen er utført i et standard oppsett for triaxial bergmekaniske målinger, med en integrert lavfrekvent modul, som gir mulighet for dynamiske målinger i det seismiske frekvensområdet. Hovedfokus i denne avhandlingen er å undersøke den dynamiske ikke-elastiske deformasjonen under reduksjon av spenning nært vendepunktet, og i tillegg sammenligne den ikke-elastisk mykheten fra dynamiske og statiske målinger. Ligninger for å sammenligne målingene er utledet, og anvendelse av modellen er demonstrert igjennom eksperimentelle resultater. Det er tydelig samsvar mellom dynamiske målinger og den ekstrapolerte linjen, og resultatene styrker ideen bak å kombinere statiske og dynamiske målinger for evaluering av elastisk spredning. Siden de lavfrekvente målingene er tatt ved bruk av strekklapper festet på kjerneprøven, var i tillegg en mulighet til å undersøke påliteligheten av en metode hvor man taper strekkmålerne på kjerneprøven. Bekymringer fra det vitenskapelige miljøet om metoden hvor man taper strekklapper i stedet for å lime dem på, førte til en beslutning om å sammenligne tapet mot limt. Sammenligningen viser liten forskjell i eksperimentelle verdier, og resultatene har en sterk sammenheng i plottene.

Acknowledgment

First and foremost, I would like to thank my supervisor Andreas Bauer. His guidance and support during the work on my thesis has been excellent. Second I would like to give an extra credit to Ph.D. candidate Serhii Lozovyi. His help in the laboratory has been truly essential for obtaining the experimental results. I would also like to thank my parents, for early making me interested in natural science and kept on challenging me during all these years in school. Finally, I would like to thank Eirik, Ørjan, Andreas, Sondre, Lars, and Haakon, for making my years as a student at NTNU joyful.

Table of contents

List of figures

List of tables

1 Introduction

1.1 Background

Wave propagation through a rock can alter the volume and deform the rock in an elastic and plastic way. The wave's ability to elastically deform the rock implies that there is a fundamental connection between rock acoustics and rock mechanics (Fjær, Holt, Horsrud, Raaen, & Risnes, 2008, p. 175). For the petroleum industry, understanding wave behaviour in a rock can give essential information and knowledge about the rock mechanical properties. The rock mechanical properties include elastic properties and non-elastic properties, and these properties can be obtained in laboratory experiments. The dynamic and static stiffness of the rock is an active field of research at the scientific community at SINTEF Petroleum Research, Trondheim, Norway. The stiffness of the rock defines the relationship between the applied stress and the resulting strain (Fjær, Stroisz, & Holt, 2013), and by combining static and dynamic measurements one has the possibility of looking into the transition from elastic to non-elastic behaviour (Fjaer, Holt, Nes, & Stenebraten, 2011). A linear growing difference between the inverse static and dynamic stiffness has been observed when decreasing stress for the unloading path (Fjaer, Holt, & Stroisz, 2012). This linear relationship, referred to as the non-elastic compliance, can be used for evaluation of elastic dispersion, which is important for calibration and interpretation of seismic surveys. Earlier experiments have not been able to measure reliable data points close to the start of the unloading because of artefacts. It requires a certain stress alteration to establish a true gradient value for the static stiffness, and the non-elastic compliance needs to be extrapolated to obtain measurements at the turning point. New equipment available has made it possible to investigate this range by comparing the extrapolated line with direct dynamic measurements. The linear relationship between the non-elastic compliance and stress is empirical, and it is believed that the Young's modulus obtained from our experiments exhibits a similar relationship as the uniaxial compaction modulus used in earlier experiments. Since the low frequency measurements are obtained from strain gauges attached on the core sample, it was possible to also include a reliability study of the method of using taped strain gauges. Concerns from the scientific community about the method of taping strain gauges instead of gluing them, led to a decision of comparing taped measurements to glued measurements.

1.2 Thesis structure

The experiments in this thesis have been performed in a standard setup for triaxial rock mechanical measurements, with an integrated low frequency module, which allow for dynamic measurements in the seismic frequency. This setup produces both static and dynamic measurement of the stiffness component of the rock. A brief introduction to acoustics and some qualitative characteristics of wave phenomena will be presented in chapter 2. An overview of the rock mechanical properties, and how the stiffness, deformation, and strain behaviour are related, will be explained in in chapter 3, together with the derivation of the equation for plotting the non-elastic compliance for dynamic measurement. Chapter 4 introduces the experimental setup and how the measurements was obtained. The relevant experimental results will be discussed in chapter 5 respectively, and the conclusion and further outlook are presented in chapter 6.

2 Acoustics

"*The wave propagations ability to travel long distances through the Earth, makes it a powerful tool for investigating the formation that otherwise would have been inaccessible"* (Fjær et al., 2008)

2.1 Introduction to acoustics

Acoustics is a classic discipline within physics that study the mechanical waves propagating through a media. Acoustic waves are often referred to as sound waves, that is because acoustics is within the frequency of the audible (Fahy, 2001). However, acoustics involves vibration, sound, infrasound and ultrasound, yet this definition can vary a bit between various fields. The mechanical waves can propagate through gas, liquid and solid, and the wave phenomena can be understood as mechanical disturbances in the media. These mechanical disturbances are time dependent changes, and involves changes in (Fahy, 2001, p. 6):

- Pressure;
- Temperature;
- Position of particles;
- Density.

Wave propagation through a rock can alter the volume and deform the rock both elastic (reversible) and plastic (irreversible). An explanation of how the deformation occur will be presented later, but the waves ability to elastically deform the rock, implies that there is a fundamental connection between rock acoustics and rock mechanics (Fjær et al., 2008, p. 175). To understand more about this relationship and the wave phenomena, it is necessary to learn more about the basic theory in wave propagation and its behaviour.

2.1.1 Wave propagation through media

When an acoustic wave passes through a material, the particles in the material are forced into an oscillating motion. Each particle has a separate volume within the material, and the oscillating motion creates a disturbance and moves the particle out of its original position.

The adjacent particle behind will then 'push' the next particle and accelerate it, and from Newton's second law of motion, it is implied that the energy must be transferred from one particle until the next. The movement is propagating from particle to particle through the material as a wave, and this will continue until the energy been attenuated and the mechanical disturbances will stop.

Acoustic waves moving through inviscid fluids only allow one type of wave. Since inviscid fluid is not able to support shear stress, the particle displacement has to move in the direction parallel to a single traveling wave (Fahy, 2001, p. 271). See illustration in Figure 2.1. This type of wave is called longitudinal wave or compressional wave, but often just referred to as the P-wave. The P-wave is an abbreviation for both pressure wave and primary wave.

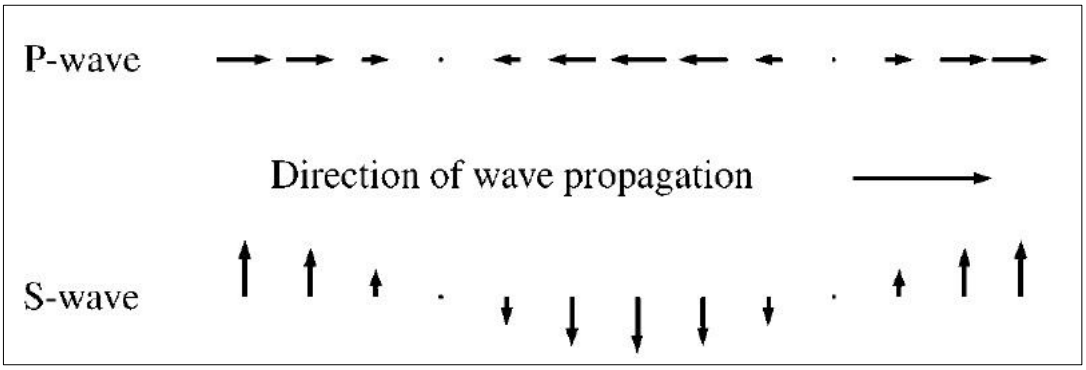

Figure 2.1 Particle displacement for P-wave and S-wave (Fjær et al., 2008, p. 179)

Solid materials on the other hand, has the ability to withstand shear stress. For an isotropic homogenous solid, both P-waves and S-waves (also called shear-wave or transversal) can exist. A combination of the P-wave and S-wave can create other types of waves like Love waves, Rayleigh waves, Stoneley waves etc. These waves have their own characteristics, but this thesis will not go into further detail, but see for instance (Rossmanith, 1978) for an overview.

For the petroleum industry, understanding wave behaviour in a rock can give valuable information. The P-wave and S-wave propagating has a certain velocity in different lithology, this give each lithology its own 'fingerprint'. By using more advanced technology, one can also differentiate between rocks, minerals, fractures, oil-water contact, dual porosity, permeability and more (E. Kozlov, 2009). The velocity of a traveling wave depends on the elasticity (stiffness) and density of the material. In seismic traces, the wave velocity is the key for understanding the underground. Therefore, it is crucial to find all the rock parameters that can help explaining wave behaviour.

2.1.2 Attenuation of waves

To understand the attenuation of waves, it is convenient to remember some qualitative characteristics of wave phenomena (Fahy, 2001, pp. 12-21).

Wavefronts

Waves generated from a monopole will propagate in all directions. If the medium is homogeneous the wave will be spread like a spherical shell, and this outer surface ('front') is known as a wavefront. This also implies that the wavefront is the first signal of the propagating wave, but do not confuse with the first or highest amplitude.

Harmonics

Repeating signals, such as sinusoidal waves. The frequency and amplitude of such a wave are repeating from the original wave source (from the fundamental frequency). The original wave is also called 1st harmonic, the following harmonics are known as higher harmonics.

Interference

Interference is evident if the wave field is analysed into many finely resolved frequencies. Interference occur if the sources are coherent or phase related. Then steady sources can create constructive ('additive') and destructive ('subtractive') interference that creates patterns of high and low sound amplitude.

Refraction & Reflection

A wave traveling from one medium to another will be refracted ('bent') and/or reflected at the interface, if there is a difference in elasticity and density between the medium, and the

angle of incident is sufficient. See Snell's law and critical angle for further understanding of when reflection occur.

Scattering

Obstacles that are much smaller than a wavelength scatter waves in all directions. Scattering of the waves results in a decrease in the amplitude, which will alternate the wavefront, the first harmonic, and the higher harmonics.

For an elastic wave the wavefront loses energy when traveling through a rock. This results in a decrease in amplitude, and over time the wave is attenuated. Attenuation occur due to geometrical spreading, scattering of wave energy, and transformation of wave energy into other forms of energy (Fjær et al., 2008, p. 185). The amplitude will reduce from its initial value by increasing the distance travelled. When the wave has travelled some distance and enters far field conditions, reduction in the amplitude is dependent of itself and will decrease exponential. Equation (2.1) show the reduction of amplitude for a plane wave traveling in the x-direction.

$$u = u_0 e^{-\alpha \cdot x} \tag{2.1}$$

Where x is equal to the travelled distance [m] and α is a measure of the attenuation [m^{-1}]. Attenuation is often displayed by the parameter Q, which is inversely proportional of α, hence decreasing Q implies an increase in attenuation. This parameter is often referred to as the quality factor, Q (see (Hoffman, 2011) for deriving of attenuation (α) and Q-factor).

$$Q = \frac{\omega}{2\alpha v} \tag{2.2}$$

ω is the angular velocity equal to $2\pi f$, and v is the wave velocity. The measured value for the Q-factor vary strongly depending on the conditions of the rock, and it is hard to obtain reliable data. Figure 2.2 shows the Q-factor versus differential pressure. An increase in Q-factor means lower attenuation for the mechanical waves.

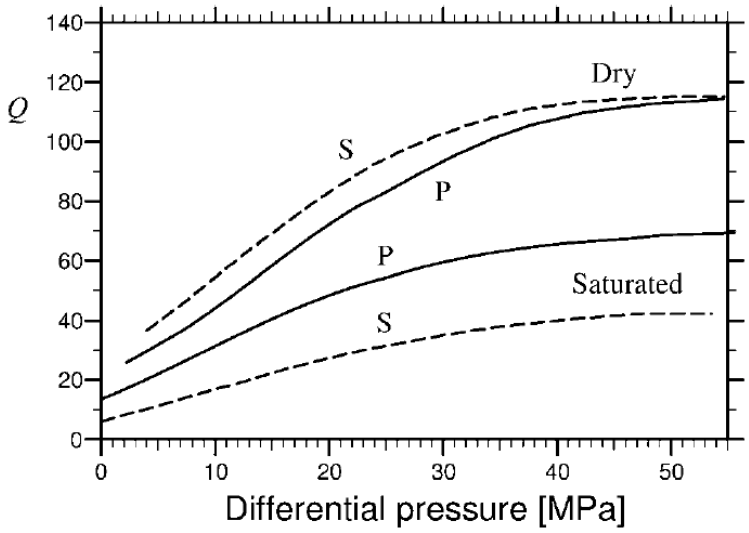

Figure 2.2 Increasing Q-value is proportional with decreasing attenuation (Fjær et al., 2008).

In the experiments carried out for this thesis, one of the largest contributor for attenuation is an effect called *local squirt flow*. Due to local variations in pore size, shape and distribution, the local strain will also vary. This results in local differences in pore pressure, which makes the pore fluid flow back and forth, following the oscillating mechanical waves. This only happens for partially and fully saturated rocks, and the attenuation is largest in a frequency range where oscillating deformation matches the characteristic relaxation time for the local squirt flow (see (Fjær et al., 2008, p. 187).

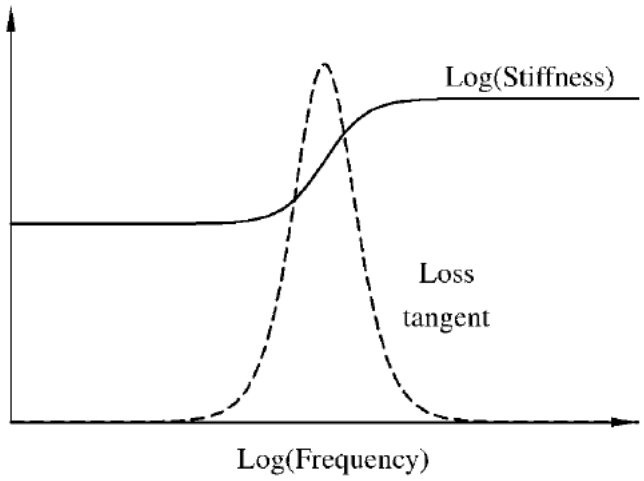

Figure 2.3 Attenuation (dashed) and stiffness against frequency ((Fjær et al., 2008, p. 187)

By comparing two different waves with the same oscillating frequency, one can see if there is any phase shift (θ) between them. Figure 2.4 illustrates the phase shift between two waves with same amplitude and frequency. In the experiments carried out, there is a measure of the oscillating wave (deformation) on aluminium and on the core sample. Aluminium is non-dispersive; therefore, it will be in the same phase as the reference input signal. The increase in the phase shift is proportional with the attenuation.

$$\mathrm{Tan}(\theta) = \frac{1}{Q} \tag{2.3}$$

The phase shift between the waves is used for interpretation of dispersion and correction of errors.

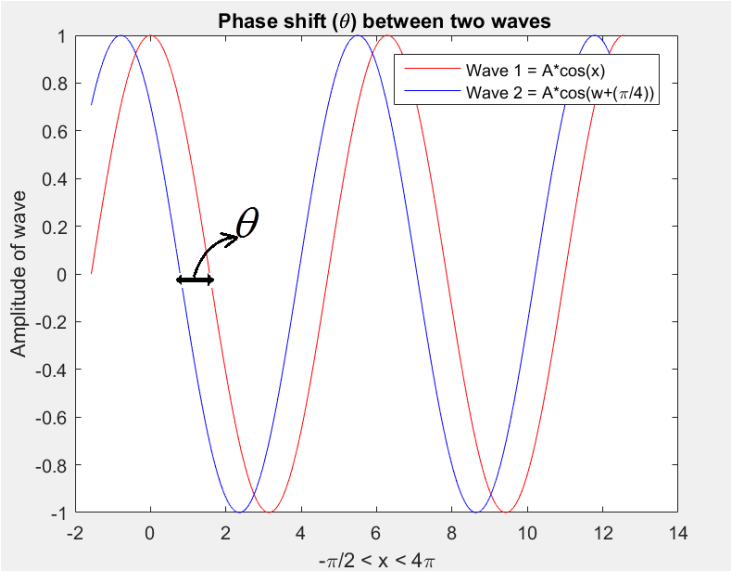

Figure 2.4 Phase shift between two waves. The reference wave is measured on a fully elastic material. Comparing this with the wave measured from the core sample will give the phase shift.

3 Rock mechanical properties

3.1 Moduli measurements in the laboratory

Measuring rock mechanical properties can give important knowledge about a rock or formation. The rock mechanical properties include elastic properties such as Young's modulus (E), Poisson's Ratio (ν), bulk modulus (K), and shear modulus (G), as well as inelastic properties which tell something about the plastic deformation and strength of the formation. This thesis will focus on measuring the mechanical properties during both a static and a dynamic test.

Static tests are done by loading and unloading of the sample. When applying a constant change in the axial loading, the linear variable differential transformer (LVDT) gives a direct measure of the deformation. The applied force is known, and by the deformation in axial and radial directions, one can calculate Young's modulus and Poisson's Ratio (α).

Dynamic tests are carried out when the loading (force) is held constant. From the lock in amplifier the amplitude and frequency are decided. Then by converting sinusoidal waves to small oscillating mechanical forces, one can measure the force applied on the core, and also the deformation in radial and axial direction. The procedure will be explained in more detail in section 4.1.

3.1.1 Linear elastic material

If the core is deformed in a way that it cannot be repositioned by tilting and/or rotating, the core sample has been 'strained'. It is not the actual deformation in radial and axial direction that is necessarily useful, but the relative displacement, i.e. the old length compared to new length of the core sample. Strain is a unit less parameter expressed by equation (3.1) (Fjær et al., 2008, p. 14).

$$\varepsilon = \frac{L_i - L_d}{L_i} = \frac{-\Delta L}{L_i} \tag{3.1}$$

L_i equals the initial length of the sample, and L_d equals the length when deformed. The relationship between the stress applied and the resulting strain is given by the sample's stiffness (Fjær et al., 2013). If the relationship is linear, the material is referred to as a linearly elastic material (see Figure 3.1). For a triaxial compression or decompression test, the relevant static stiffness of the rock sample is the Young's modulus (E) (Fjaer et al., 2011). By assuming no anisotropy, one can calculate Young's modulus by using equation (3.2).

$$E = \frac{\sigma_{axial}}{\varepsilon_{axial}} = \frac{\sigma_x}{\varepsilon_x} \tag{3.2}$$

Young's modulus is part of the group called elastic moduli. The applied stress in a triaxial compression test will also deform the core sample in width. The strain ε_y and ε_z describes the elongation in y- and z-direction, i.e. they describe the alteration in cross-section area of the sample. By assuming $\varepsilon_y = \varepsilon_z$, the Poisson's ratio (ν) can be found by equation (3.3).

$$\nu = -\frac{\varepsilon_y}{\varepsilon_x} \tag{3.3}$$

Poisson's ratio (ν) is a measure of the lateral expansion relative to longitudinal contraction, and it is another elastic parameter. Both Young's modulus and Poisson's Ratio can be found by measuring the stress and obtaining the strain from experiments in the laboratory. The stress and strain relationship are the foundation of deriving equations for isotropic, linear elastic materials (Fjær et al., 2008). By obtaining Young's modulus and Poisson's Ratio you can calculate other elastic moduli such as bulk modulus (K) and shear modulus (G).

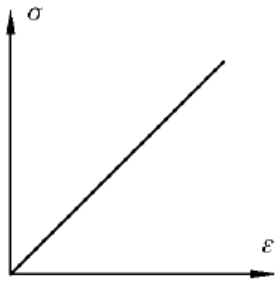

Figure 3.1 Stress - strain relationship for elastic core sample (Fjær et al., 2008).

3.2 Nonlinear elastic to non-elastic

If the strain increases or decreases nonlinear, the material will not behave linear elastic (Fjær et al., 2008, p. 42). The stress-strain curve from Figure 3.1 will be different and no longer have a linear trend. For a nonlinear perfectly elastic behaviour, the stiffness will be depending on the stress alteration (see Figure 3.2). The change in stress can be expressed by equation (3.4).

$$\Delta\sigma = E_{\tan}(\sigma) \times \Delta\varepsilon \tag{3.4}$$

$E_{\tan}(\sigma)$ is the tangent value of the Young's modulus (Fjær et al., 2008, p. 43). If the loading path is different from the unloading path, the stress-strain curve will follow the pattern of hysteresis. In Figure 3.2, one can see that the plot in the middle forms a hysteresis loop.

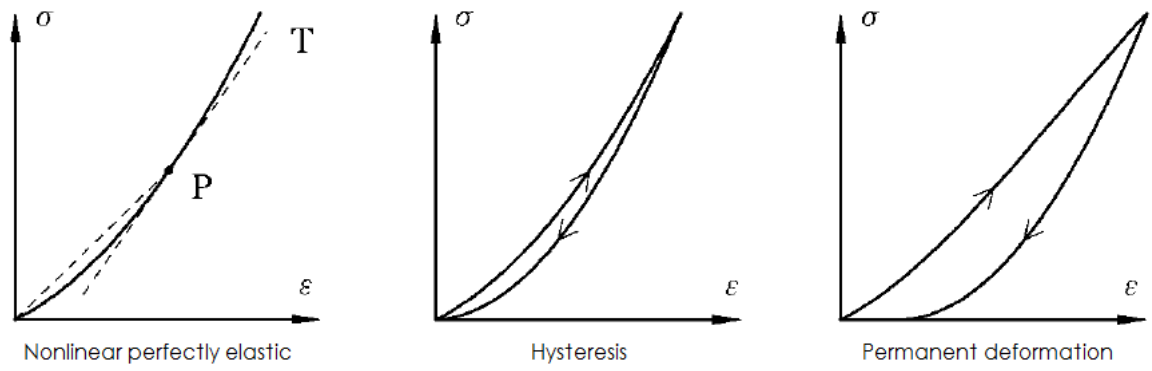

Figure 3.2 Nonlinear elastic to non-elastic stress-strain behaviour (Fjær et al., 2008, p. 42)

The hysteresis is observed because of plastic effect during loading and unloading. If some of the deformation is permanent, the material is said to have reached its yield point. The yield point is the transition from elastic to ductile behaviour. Materials exposed for stress beyond the yield point typically suffer plastic deformation, i.e. permanent deformation and the curve in the stress-strain plot can behave in many different ways. The hysteresis loop in Figure 3.2 can be a bit misleading. If the strain really goes back to zero, the material is elastic, but in most cases the hysteresis would cause plastic deformation. The start of the unloading is typically not zero, and could already be affected by plastic deformation.

3.2.1 Non-elastic response

As presented in the introduction, the purpose is to use the dynamic measurement to investigate the linear relationship between the non-elastic compliance and the stress, a method created by scientists (Fjær et al.) from SINTEF, Trondheim, Norway. The method is based on results from earlier experiments, and those experiments have not been able to measure reliable data points in the beginning of the unloading. This is due to experimental artefacts, and the range from the turning point until a certain stress alteration has been extrapolated based on the plot for the non-elastic compliance (Fjær et al., 2013). By utilizing the dynamic measurement, it is possible to investigate in this extrapolated range. The dynamic low frequency measurement cannot be plotted directly as a continuous function, which is the case for the static measurement. Therefore, the dataset needs to be integrated if to be compared. Before looking into the integration limits, the function for the static stiffness should to be presented.

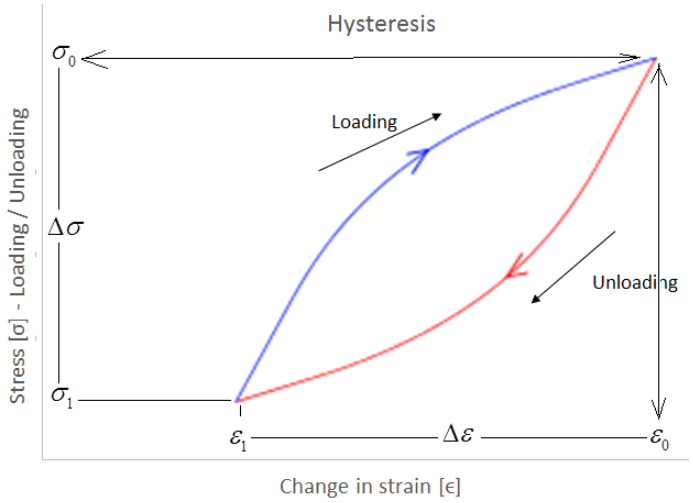

Figure 3.3 Hysteresis in the stress-strain plot. Unloading path: Integration limits for the dynamic measurement

The function for the static stiffness is found from the angle of inclination from the stress-strain plot. See Figure 3.3. The static stiffness is the derivative of the unloading path; $E = d\sigma / d\varepsilon$. Since earlier experiments are carried out using a standard setup for uniaxial rock mechanical measurements, the measured stiffness is a bit different than Young's

modulus. For a uniaxial compaction test (K_0 test), where the lateral deformation is kept constant, the static stiffness component is expressed by equation(3.5):

$$H = \frac{\Delta\sigma_z}{\Delta\varepsilon_z} \tag{3.5}$$

where H is called the static uniaxial compaction modulus. For a linearly elastic material, where the rock is homogenous and non-dispersive, corresponding static and dynamic modulus are equal. For heterogeneous material such as porous rocks there may be a large difference (Fjær et al., 2013). For comparison, it is convenient to define the non-elastic compliance S_H shown in equation (3.6).

$$S_H = \frac{1}{H} - \frac{1}{H_e} \tag{3.6}$$

This is an empirical equation derived from the results of the uniaxial compaction modulus. It is assumed that the Young's modulus exhibits a similar relationship as the uniaxial compaction modulus. Out of respect of previous work, the equations will be presented as they were originally, before substituted to match the parameters in this thesis. The non-elastic compliance appears to increase linear for unloading in uniaxial compaction test (Fjaer et al., 2012), except at the very beginning where $H = H_e$. For non-dispersive materials, the starting point for the non-elastic compliance is zero:

$$S_H = \frac{1}{H} - \frac{1}{H_e} = a(\sigma_z^0 - \sigma_z) \tag{3.7}$$

where a is a constant, and σ_z^0 is the initial stress before unloading. In the earlier experiments, the dynamic stiffness was obtained from the ultrasonic measurement. For a uniaxial compaction test, the dynamic uniaxial compaction modulus is expressed by the density (ρ) and axial P-wave velocity (V_p) in equation (3.8) (Fjaer et al., 2011) (Fjaer et al., 2012).

$$H_e = \rho \times V_p^2 \tag{3.8}$$

If the rock is dispersive, the axial P-velocity will be different at low frequency (1-2 Hz) compared to ultrasonic frequency (500k Hz). The static measurement can be compared to a frequency in the range of 1 Hz, and since $V_{P,low} \neq V_{P,ultrasonic}$, then $H \neq H_e$. This implies that at the beginning, the non-elastic compliance should not be equal to zero, but have a starting value equal to the constant b.

$$S_H = \frac{1}{H} - \frac{1}{H_e} = a(\sigma_z^0 - \sigma_z) + b \tag{3.9}$$

Figure 3.4 show the linear growth of the non-elastic compliance with the starting point b. The linear relationship from equation (3.9) is used to extrapolate the non-elastic compliance, to the vicinity of the start of the unloading path (Fjaer et al., 2012).

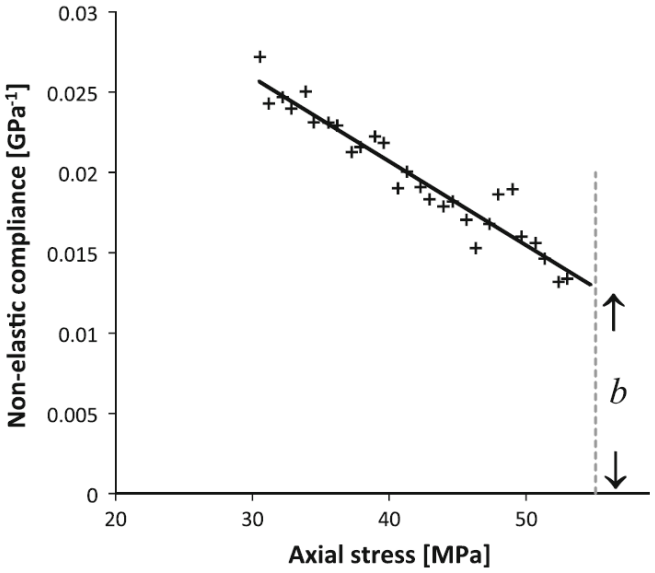

Figure 3.4 Non-elastic compliance (Fjær et al., 2013).

Since the low frequency can measure the strain and stress at low values, it is possible to obtain data points close to the turning point. This thesis will run the low frequency measurements at 2 Hz, therefore the dispersion effect will be low and $b \to 0$, as in equation (3.7). Since it is assumed that Young's modulus exhibits a similar relationship as the uniaxial

compaction modulus H, it is possible to introduce Young's modulus in equation (3.7). Rearranging equation (3.7) and substituting with Young's modulus will give equation (3.10):

$$\frac{1}{E} = S_E + \frac{1}{E_e} = a(\sigma_z^0 - \sigma_z) + \frac{1}{E_e} \tag{3.10}$$

where $1/E_e$ is to be assumed constant for the relative small stress changes of interest. As seen in Figure 3.3, the static stiffness is the derivative of the unloading path; $E = d\sigma / d\varepsilon$. Then the non-elastic compliance for the static measurement can be plotted by equation (3.11):

$$\frac{1}{E} = \frac{d\varepsilon}{d\sigma} = a \times \Delta\sigma + \left(\frac{d\varepsilon}{d\sigma}\right)^{el,0} \tag{3.11}$$

where $\Delta\sigma = (\sigma_z^0 - \sigma_z)$ and $d\varepsilon / d\sigma = 1/E_e$. Since the low frequency is a dynamic measurement, the data points are not a continuously static function, and the dataset needs to be integrated if to be compared. Then integrating equation (3.10) with the same limits as in the Figure 3.3:

$$\int_{\varepsilon_0}^{\varepsilon_1} d\varepsilon = \int_{\sigma_0}^{\sigma_1} \left(a \times \Delta\sigma + \left(\frac{d\varepsilon}{d\sigma}\right)^{el,0} \right) \cdot d\sigma \tag{3.12}$$

$$\frac{\Delta\varepsilon}{\Delta\sigma} = \frac{a}{2} \times \Delta\sigma + \left(\frac{d\varepsilon}{d\sigma}\right)^{el,0} \tag{3.13}$$

The lock-in amplifier measure the signals as root mean square (RMS) values. If the waveform is a pure sine wave, then the peak-to-peak (amplitudes) have a fixed relationship. Peak-to-Peak for a sine wave will give $\Delta\sigma = 2 \times \sqrt{2} \times \Delta\sigma_{rms}$ and $\Delta\varepsilon = 2 \times \sqrt{2} \times \Delta\varepsilon_{rms}$. Substituting $\Delta\sigma$ and $\Delta\varepsilon$ in equation (3.13), will give the equation for the non-elastic compliance for the low frequency measurements.

$$\frac{\Delta\varepsilon_{rms}}{\Delta\sigma_{rms}} = \sqrt{2} \times a \times \Delta\sigma_{rms} + \left(\frac{d\varepsilon}{d\sigma}\right)^{el,0} \tag{3.14}$$

3.2.2 Investigating stress dependence of elastic stiffness

The last section introduced how the non-elastic response can create the hysteresis effect in a stress-strain plot. The tangent value of Young's modulus $E_{\tan}(\sigma)$ from equation (3.4) can be linearized by taking small steps for the stress alteration.

$$E(\sigma) = E_0(\sigma) + \frac{dE}{d\sigma} \times \Delta\sigma_{ax} = E_0 + A \times \Delta\sigma_{ax} \tag{3.15}$$

A is a constant that depends on the slope. In equation (3.15) it is assumed that $E_0(\sigma)$ is independent of stress, and can be written as a constant E_0. In Figure 3.2 it was seen that the hysteresis effect cannot be created by just nonlinear elastic deformation. Let's assume the stress changes as a harmonic sinusoidal wave, then because of symmetry, the second harmonic only affect the nonlinear elastic behaviour when loading and unloading. Then $E(\sigma)$ has the same absolute value at the beginning of the unloading as at the beginning of the loading, and it is believed this is due to translational symmetry for the even harmonics. From Figure 3.5, one can see that the first (odd) harmonic behaves asymmetric over half a period, while the second (even) harmonic has continuously translational symmetry.

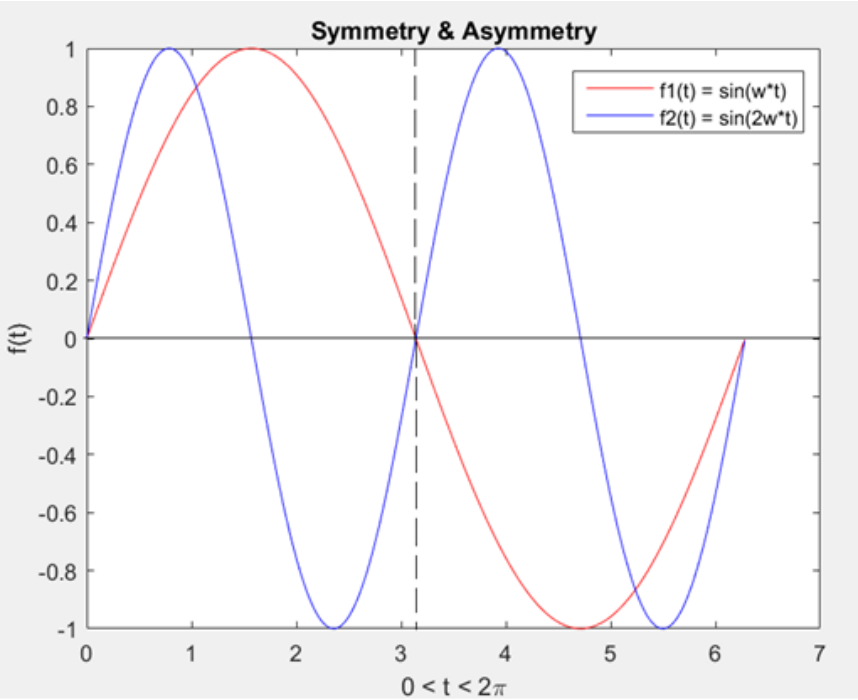

Figure 3.5 Symmetric and asymmetric sinusoidal waves. The red function is the first harmonic and the blue is the second harmonic.

For the first function in Figure 3.5, the first half of the period T equals minus the other half.

$$f(t) = -f\left(t + \frac{T}{2}\right) \tag{3.16}$$

This is the representation for the anti-symmetric case ((Connell, 2004). For the first harmonic, it can easily be seen that the sinusoidal wave, $\sin(\omega \times t)$, satisfy equation (3.16).

$$\sin(\omega(t + \frac{T}{2})) = \sin(\omega \times t + \pi) = -\sin(\omega \times t) \tag{3.17}$$

Where the period $T = 2\pi / \omega$. In Figure 3.6 one can see how the first harmonic will deform the material depending on the time period.

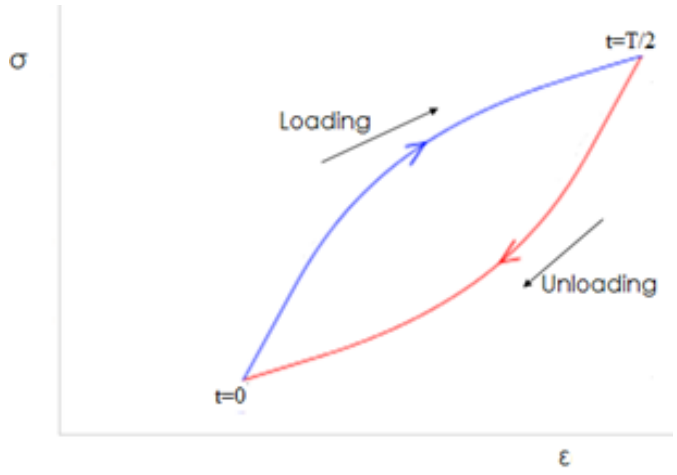

Figure 3.6 Stress – strain curve depending on the time.

For the second harmonic one can see from Figure 3.5 that the integrated function over half a period will cancel the overall contribution. Translational symmetry can be represented as the function in equation (3.18).

$$f(t) = f(t + \frac{T}{2}) \tag{3.18}$$

By showing that the second harmonic can fit equation (3.18), the second harmonic needs to be integrated over the period T.

$$\int_0^T f(t)dt = \int_0^T \cos(2\omega t)dt = \int_0^{T/2} \cos(2\omega t)dt + \int_{T/2}^T \cos(2\omega t)dt \quad (3.19)$$

Then the last term is the second half of the period T and can be rewritten:

$$\int_{T/2}^T \cos(2\omega t)dt = \int_0^{T/2} \cos(2\omega(t' + \frac{T}{2})dt = \int_0^{T/2} \cos(2\omega(t' + \frac{\pi}{\omega})dt \quad (3.20)$$

where $t \Rightarrow t' + T/2$. Substituting this into equation (3.19):

$$\int_0^T \cos(2\omega t)dt = \int_0^{T/2} \cos(2\omega t)dt + \int_0^{T/2} -\cos(2\omega t)dt = 0 \quad (3.21)$$

and remember $\cos(2\omega t + 2\pi) = -\cos(2\omega t)$. It can now be seen that the second harmonic has translational symmetry as in equation (3.18).

$$\int_0^{T/2} \cos(2\omega t)dt = \int_0^{T/2} \cos(2\omega(t + \frac{T}{2})dt \quad (3.22)$$

The second harmonic will be absent to any non-elastic effect. However, if $E_0(\sigma)$ is stress dependent, equation 3.15 is not valid, and the translational symmetry is broken. The tangent value $E(\sigma)$ will not be the same at the beginning of the unloading as at the beginning of the loading. The hysteresis loop will then be different, as shown in Figure 3.7 as dashed curves.

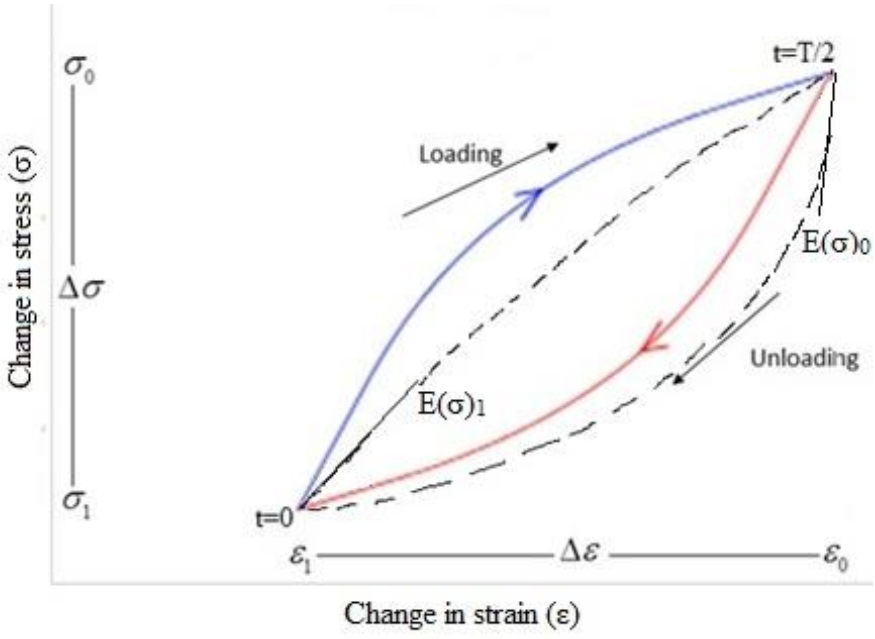

Figure 3.7 Hysteresis loop. The dashed hysteresis is the case where the symmetry is broken. Notice $E(\sigma)_0 \neq E(\sigma)_1$.

By utilizing the higher harmonics, it is possible to investigating the stress dependence of elastic stiffness. This is a scientific field that has limited experimental data. $E_0(\sigma)$ is stress dependent in Figure 3.7. The symmetry is broken and it can be seen that $\left|E(\sigma)_0\right| > \left|E(\sigma)_1\right|$. The last experiment in this thesis investigated the second harmonic, and the results will be presented in chapter 5.

4 Experiments

4.1 Experimental measurements

The experiments were performed in a standard setup for triaxial rock mechanical measurements, with an integrated low frequency module and ultrasonic transducers inside the top and bottom endcaps. The measurements for the low frequency setup is at seismic frequencies (1 Hz – 155 Hz). The setup allows for axial loading on the core, and since a pump is connected, it can increase the confining pressure around the core. A pore-fluid line is connected at the top and bottom of the endcaps, used to saturate and regulate the pore pressure for the sample. The experiments can be run dry, or under drained and undrained conditions. Figure 4.1 shows a schematic of the setup around the core, and a picture of the actual setup. Notice that the vessel covering the core is missing in both cases.

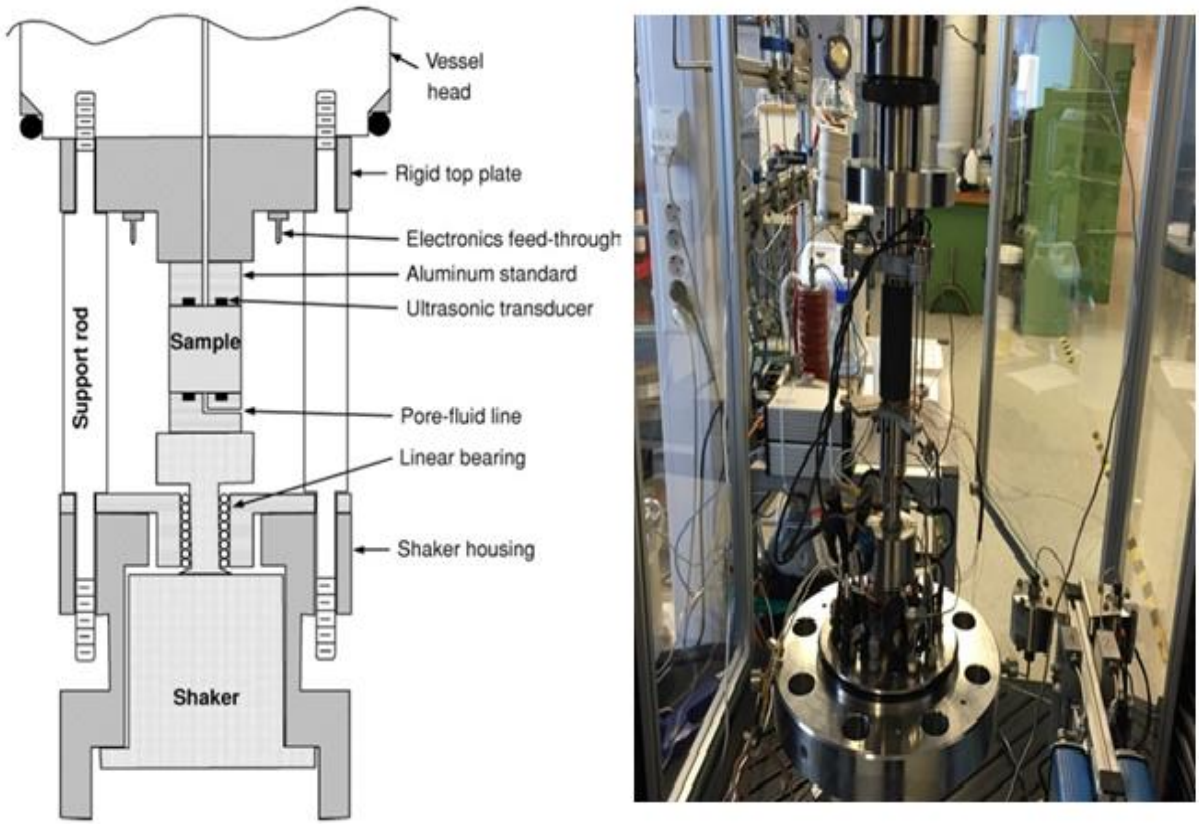

Figure 4.1 Left: Schematic of the lowfrequency assembly (Batzle & Hofmann, 2006). Right: Picture of the assembly without the vessel around it.

The schematic in Figure 4.1 is a bit different from the actual setup. In the experiments, the shaker was replaced by piezoelectric actuators (crystals). For the low frequency setup, the first step in the 'cycle' of obtaining measurements begin in the master lock-in amplifier. The master sends electric signals which is then amplified before they are sent to the assembly. The master lock-in amplifier also decides what frequency and sinusodial wave amplitude to be used. The master tells the slaves (rest of the lock-in amplifiers) what frequency to be locked into, which enable the slaves to remove the noise from other frequencies. The slaves are measuring radial or axial strain. See Figure 4.2 for an overview. The spesific frequency and wave amplitude are sent to an amplifier that amplifies the signal. The sinusoidal electric signals are then converted by the piezoelectric actuator into mechanical waves.

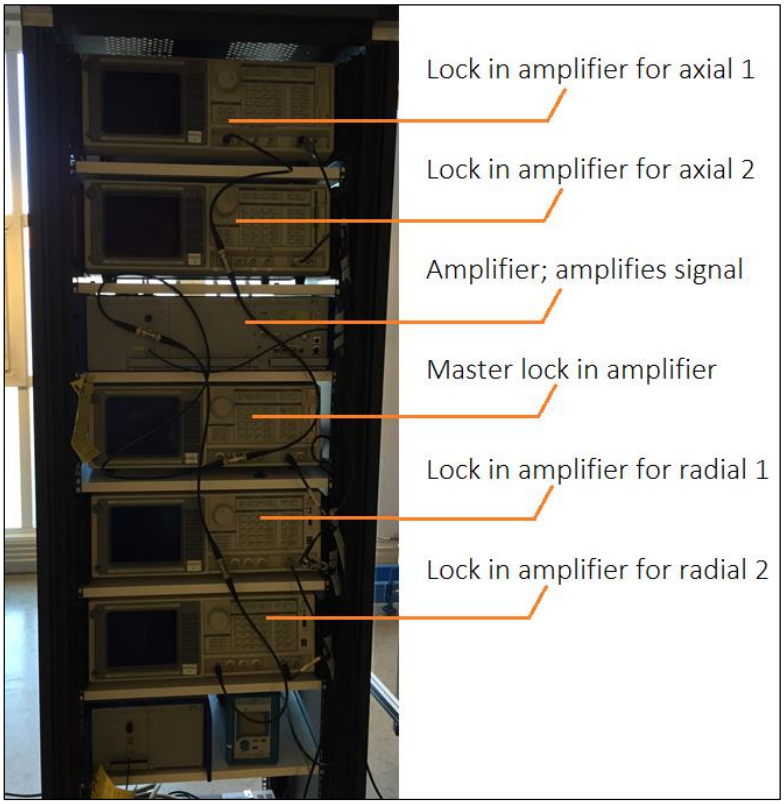

Figure 4.2 Overview of the lock-in amplifiers.

The mechanical waves works as small force amplitudes on the core sample, and the core will have some small oscillating deformations. At the other side of the core is another piezoelectric actuator, and it will generate charges at the surface when exposed to

mechanical deformations. These charges are then transformed in a charge meter into volt signals. The master lock in amplifer reads the electrical signals and display them as the voltage force applied. The voltage can later be converted to mechanical load for calculations. Figure 4.3 shows a simplified drawing of the 'cycle' for measuring the force.

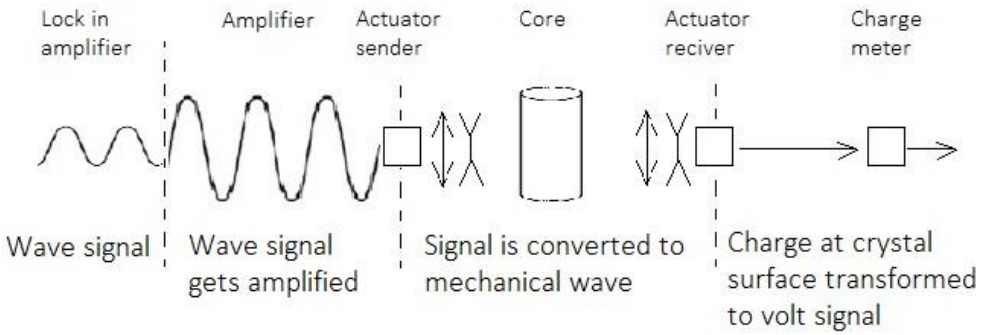

Figure 4.3 Overview of the process for measuring force applied on the core during dynamic test.

4.1.1 Strain gauges

This section will explain how the strain gauges take measurements. The strain is obtained from four strain gauges attached to the core sample. The strain gauges have a lattice structure of small wires, and since they are attached to the core, the lattice structure will deform as the sample gets compressed. Electricity is sent through the conductive lattice structure. Consider charges moving in the same direction as the electric current. Then the current through the cross-sectional area A of the wire has to be the net charge through the area per unit time (Kramer, 2012, p. 821):

$$I = q \times \eta \times v_d \times A \times dt \tag{4.1}$$

where q is the charge and v_d is the drift velocity. The current density is then the electric current divided by the cross-section area of the conductive wire.

$$J = \frac{I}{A} \tag{4.2}$$

An electric field E inside the wire is pointed in the same direction as the current (see Figure 4.4). Then the resistivity of a material can be expressed by equation (4.3).

$$\rho_R = \frac{E}{J} = \frac{E}{I} \times A \tag{4.3}$$

From Figure 4.4 one can see that the total potential over the length L is equal to $V = E \times L$. By combining equation (4.3) and the difference in potential, the total potential V can expressed in terms of the current and resistivity (Kramer, 2012, pp. 823-825).

$$V = \frac{\rho_R \times L}{A} \times I \tag{4.4}$$

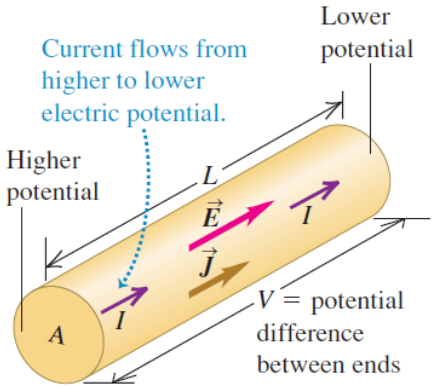

Figure 4.4 Uniform cross section and current density (J) is uniform over any cross section. Electric field (E) is then constant at any length (Kramer, 2012, p. 825).

If the electric field (E) is uniform and the current density J is constant, then from equation (4.3) one can see that the resistivity of the material ρ_R also becomes constant. The total current I in equation (4.4) is then proportional with the potential difference V. The ratio of V over I is the resistance R of a conductor (also known as Ohm's Law) (Kramer, 2012, pp. 824-826).

$$R = \frac{V}{I} = \frac{\rho_R \times L}{A} \tag{4.5}$$

From equation (4.5) one can easily see that if the cross-section area of the wires increases, the resistance will decrease. This will happen if the sample is compressed so that the wires widens. The strain gauges measure this resistance R, but the master lock in amplifier cannot read these measurements. Therefore, the measured resistance is sent to a Wheatstone:

bridge and converted to a voltage measurement (signal). The Wheatstone bridge is used to measure an unknown resistance in an electrical circuit, but in this case the resistance is known, and therefore it is possible to calculate the voltage out signal. Figure 4.5 show a sketch of a Wheatstone bridge. By using a setup like this, and the theory from Ohm's Law (4.5), one can calculate the potential difference (V) over the 'bridge':

$$V_{out} = V_{in} \times \frac{\frac{\Delta R}{R}}{2 + \frac{\Delta R}{R}} \tag{4.6}$$

Where V_{in} is the voltage into the Wheatstone bridge. The derivation of equation (4.6) can be found in appendix A, but notice from Figure 4.5: $R_1 = R_3 = R + \Delta R$ and $R_2 = R_4 = R$. Each of the strain gauges measure both axial and radial deformation, and there are four Wheatstone bridges converting the resistance to a voltage signal. The signal is then sent to the lock-in amplifiers (see Figure 4.2 for axial and radial amplifiers). By rewriting equation (4.6) and using the relationship $R / \Delta R = \varepsilon \times GF$ one can derive the equation for the strain.

$$\varepsilon = \frac{2V_{out}}{GF \times V_{in}} \tag{4.7}$$

GF is the gauge factor given by the factory to each single package of strain gauges. The derivation of equation (4.7) can be found in appendix A.

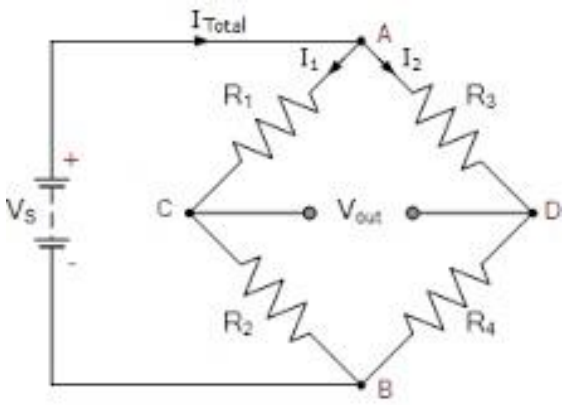

Figure 4.5: Wheatstone Bridge. Picture from Wikipedia

The master lock-in amplifier measures the force voltage amplitude out from the core, and the stress σ is obtained by using equation (4.8):

$$\sigma = \frac{F}{A} \tag{4.8}$$

where F equals force amplitude [V] times sensitivity [N/V], and A is the cross-section area of the core sample (Fjær et al., 2008, p. 2). The sensitivity can be regulated, but in reality this is usually held constant, so the force amplitude is the only thing varying the stress. From the stress and strain one can calculate the Young's modulus and Poisson's Ratio. For a standard static test the deformation is obtained from the LVDT's, and the strain gauges is not needed. By deciding a reference value for the LVDT's when the test start, the total change measured within this time span will be equivalent to the strain. The stress is obtained from the loading / unloading.

4.2 Preparations

All experiments were performed on a Castlegate Sandstone, and the preparation did not change much, except taping and gluing on the strain gauges. As mentioned in the introduction, scientists from other organisations and universities have concerns about the reliability of the method of only taping the strain gauges. Therefore, it was decided to compare glued gauges versus taped gauges. The main purpose in the laboratory was still to investigate the nonlinear elastic and the non-elastic behaviour of the stiffness of the rock.

4.2.1 Preparing core

The grains in the Castlegate sandstone is not strong enough the keep the strain gauges in place, and the grains can damage the lattice structure in the gauges, resulting in non-usable measurements (artefacts). Therefore, a layer of epoxy is used to cover the area where the gauges are attached. The area needs to be thin, smooth and as small as possible, so the strain gauges are measuring the properties of the core sample instead of the properties of the epoxy. When finished preparing the core, it is marked and weighted before being put into the oven for drying.

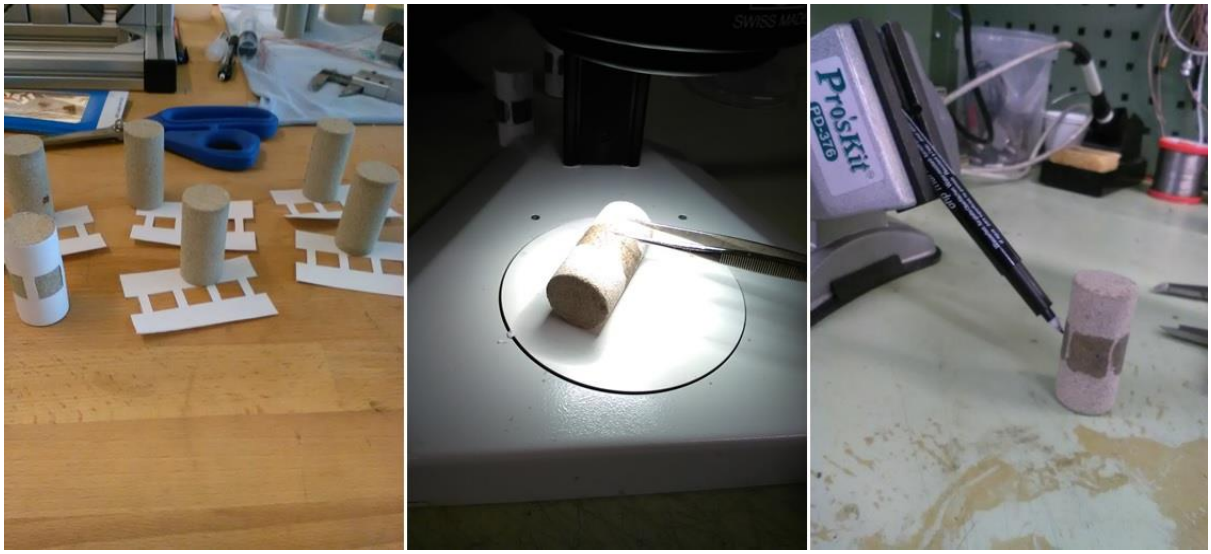

Figure 4.6 Preparing core sample. Left: Thin print to cover the sample before applying epoxy. Middle: epoxy layer is investigated and polished under microscope. Right: Marking where to put the strain gauges on the epoxy layer.

4.2.2 Strain gauges

Preparing strain gauges can be time consuming in the beginning, and it is trickier than preparing the core for someone who is inexperienced in soldering. In Figure 4.7 one can see some of the steps one need to undergo before the strain gauges are ready to use. It is important that the surface around the connection between the wires and the strain gauge is nonconductive.

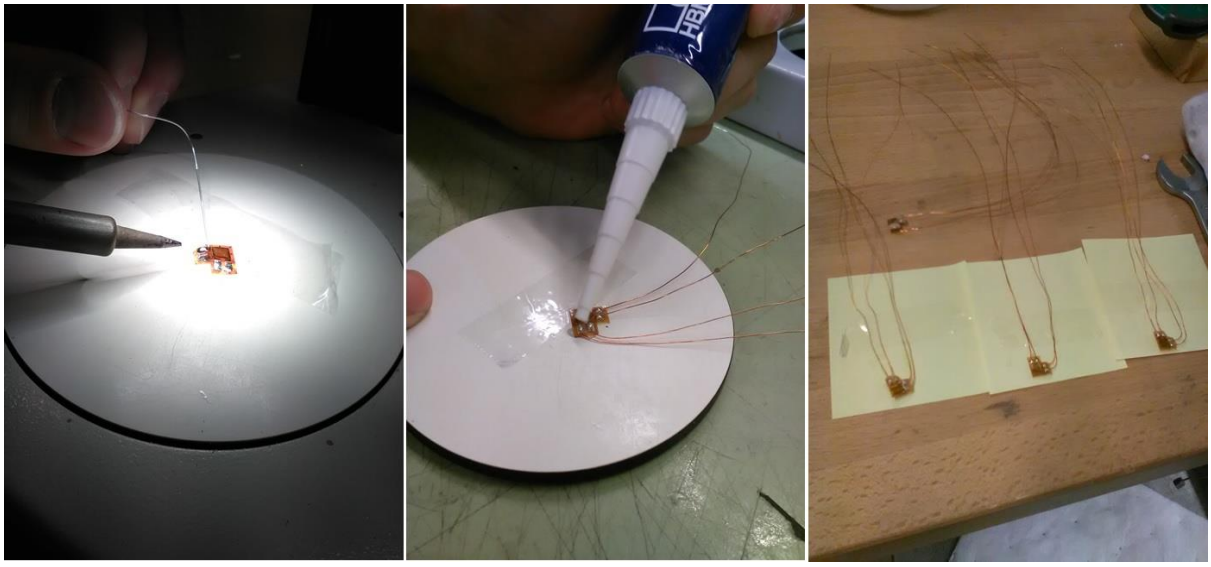

Figure 4.7 Preparing strain gauges. Left: Solder the wires unto the strain gauges. Middle: applying epoxy or silicon to protect and make the connections nonconductive. Right: four strain gauges ready to use.

Preparing core sample and strain gauges are a relatively easy task, but one can save much time by doing it properly and cautiously the first time. It is a fundamental part of the experiment, and a careful preparation can eliminate experimental failures and improve results.

4.2.3 Taped versus glued

The first experiment was to test the method were the strain gauges are taped to the epoxy, and the second experiment was to test with the strain gauges glued onto the epoxy. Taping the strain gauges onto the core has some advantages:

- Time saving;
- Easier procedure;
- Can remove strain gauges and reuse the core sample if gauges are damaged;
- The core sample is exposed to air as little as possible.

It is important to have a strong coupling between the core and the gauges; the resulting strain on the core needs to be the same for the gauges. The gauges can slip which results in no correlation in the strain. For a fully saturated core, a thin layer of pore fluid can get between the sample and the gauges, and concerns and challenges are definitely highest in such a test. Therefore, it was decided to perform both experiments fully saturated. The

results from the experiments will also give the opportunity to look into the sensitivity for acoustic frequencies measured.

4.3 Carrying out the experiment

The stress path for both glued and taped test is shown in Figure 4.8, and values are given in Table 4.1. The experiments were carried out on the same core, and the core was dried in the oven before both experiments. This was done so measurement #1 could be performed under dry circumstances. The rock sample can become a bit stiffer from the first experiment. Drying the rock can also somewhat 'reset' this effect, and make the rock more soft because small cracks can be created (Chenevert, 1997).

Table 4.1 Values for the stress path. The axial loading is shown as σ_{ax} and confining pressure as P_{conf} .

$Measurement$	$Category$	σ_{ax}	σ_{ax}	P_{Conf}	P_{Pore}	$Comments$
#	-	[N]	[MPa]	[MPa]	[MPa]	-
1	Dry	4372,0	8,89	6,89	0	Open valve
2	Saturated	5355,6	10,89	8,89	2	Open valve
3	Saturated hydrostatic	7814,6	15,89	13,89	-	Undrained / Closed valve
4	Saturated	5355,6	10,89	8,89	-	Undrained / Closed valve

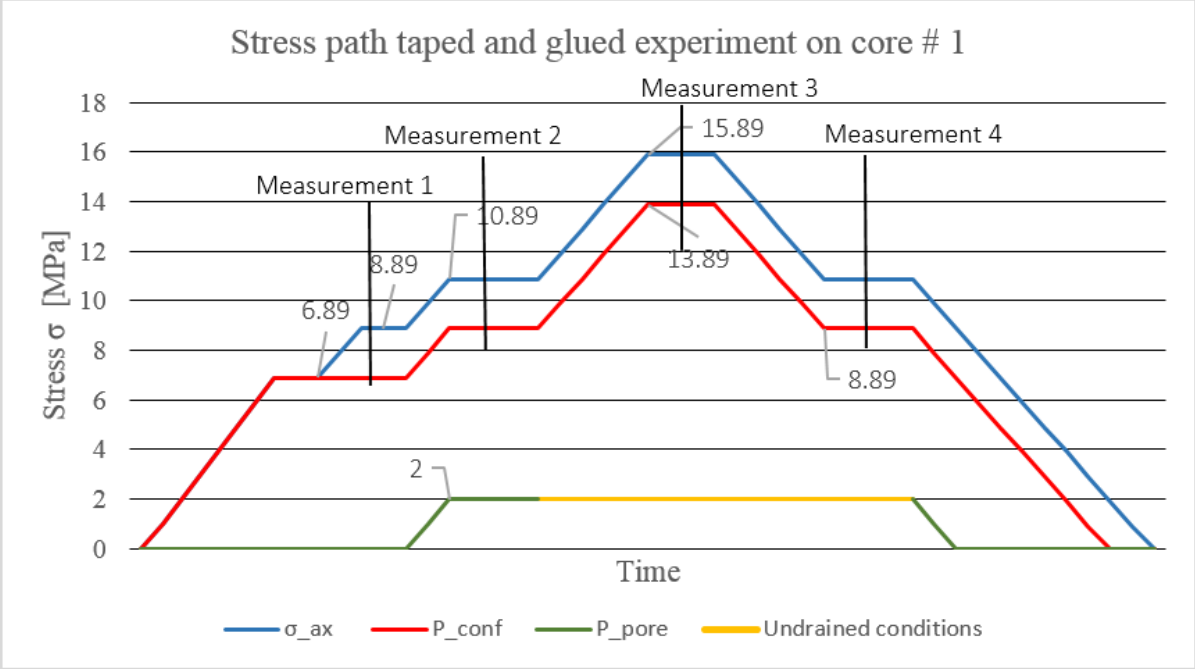

Figure 4.8 Stress path for taped and glued experiment.

4.3.1 Third experiment

The third experiment investigated the stress dependence of elastic stiffness and the non-elastic behaviour. Increasing the sine output will make it possible to investigate the non-elastic compliance, and compare it with static measurements as shown in section 3.2.1. Increasing the sine output will also make it possible to look at the contribution from the higher harmonics, regarding stress dependence.

The low frequency measurement for the dynamic strain was taken when the core was under undrained hydrostatic conditions at 19 MPa. The static strain was measured when unloading the axial stress from 19 MPa to 14 MPa.

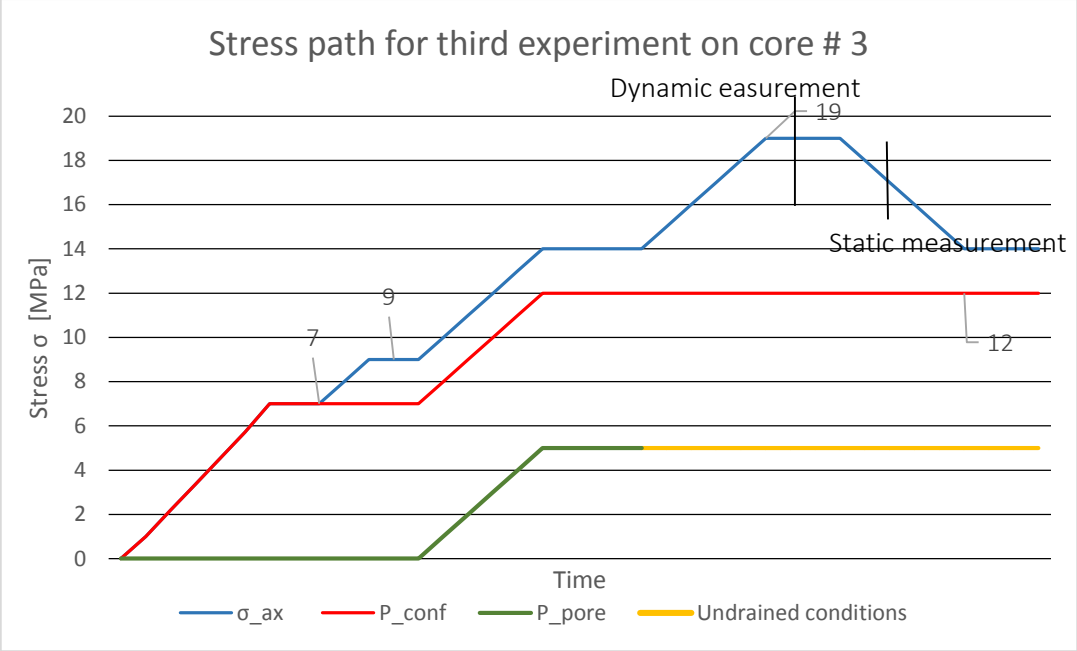

Figure 4.9 Stress path third experiment. Another student continued experiment after the static measurement.

The frequency was fixed at 2 Hz, and the sine output started at 0,1 V_{rms} and went up to 4,5 V_{rms}. Measurements for the first and second harmonics were taken for 7 different sine outputs. Then at the highest amplitude, the strain gauges measuring first and second harmonic switched, and the measurement was repeated. Then all four strain gauges measured both first and second harmonic, and the measurements end up becoming the average of the two of them. Because of surprisingly high values for the second harmonic, it was decided to look at the second harmonic on a PEEK core. PEEK is an elastic material and in theory, the second harmonic should be absent or at least close to zero.

5 Results and discussion

In this chapter all the results from the laboratory experiments will be presented. The chapter will be divided into two parts, the taped versus glued strain gauges, and the non-elastic compliance. For simplicity for the reader, observations and a discussion are presented together with the results in the end of each section. The sensitivity analyses will mainly be centred around Young's modulus measurements, and will be presented after the comparison of taped versus glued strain gauges. The excel files are excluded, if they are of interest contact the author for the files.

5.1 Taped and glued strain gagues

5.1.1 Comparing results of Poisson's ratio and Young's modulus

Figure 5.1 show the comparison of Poisson's ratio. The dry measurements are excluded in the plot, even though the measurements show strong correlation. This is because the value for dry measurement is quite low compared to the saturated, and adjusting the axis to make the data points fit makes the plot difficult to read. In Figure 5.2 one can see the comparison of Young's modulus. The dry measurement is included in this figure. The highest frequency measurements (95 Hz & 155 Hz) are an artefact, most likely because of resonance. These measurements were excluded for the comparison for both Poisson's ratio and Young's modulus.

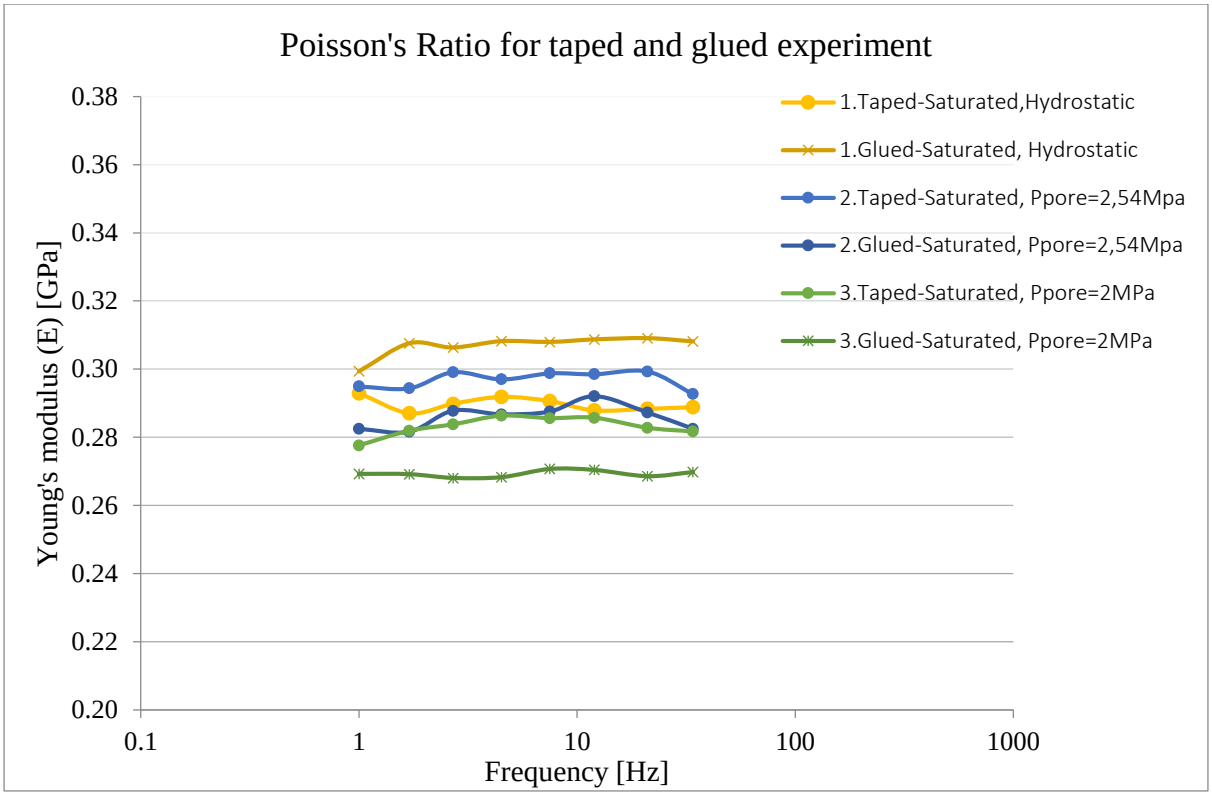

Figure 5.1 Compering Poisson's ratio. Line between measured points included for easier keeping track.

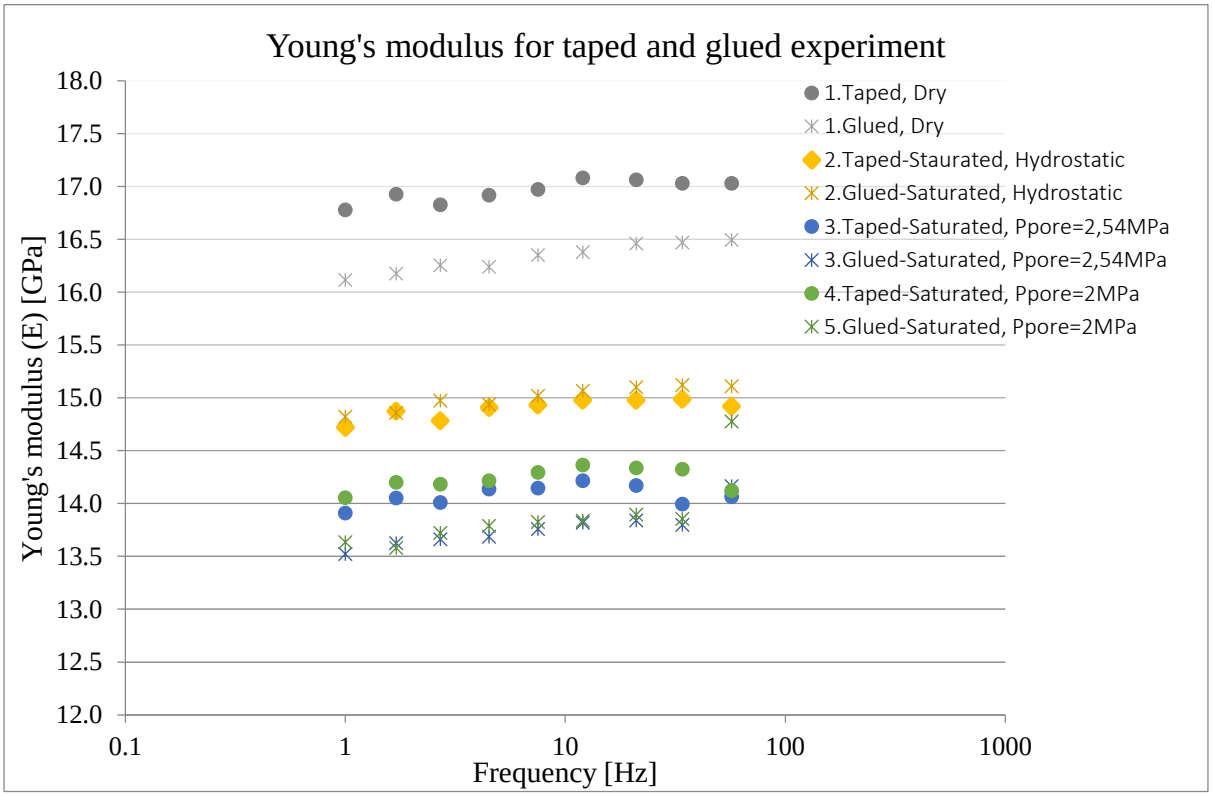

Figure 5.2 Compering Young's modulus.

Observations

Comparing the Poisson's ratio in Figure 5.1 can be confusing at first eyesight. The trend line for Poisson's ratio is not necessarily flat, and the uncertainties are often higher than the measurements for the Young modulus. Poisson's ratio also has a higher difference between dry and saturated measurements. When saturating the core, it becomes softer and the Poisson's ratio can increase to a value of about 0,5 depending on the lithology (Cregger & Lamb, 1984). The dry measurement was around 0,1 (excluded). In Figure 5.1 one can see that the saturated measurements are around 0,3, which shows an increase in Poisson's ratio of approximately 0,2.

It can be seen in Figure 5.1 that measurement number 2 and 3 have a higher value for taped compared to glued. The trend line for both measurements follow each other, especially number 2 where they behave nearly parallel. The conclusion will mainly be focused on the Young's modulus, but worth notifying a strong correlation between the taped and glued measurement for Poisson's Ratio.

Figure 5.2 show the comparison of four measurements for both glued and taped. Measurement number 2 and 3 have a slightly higher Young's modulus for the taped compared to the glued, and the data points have a similar trend. This is the same as for the Poisson's ratio. Can also observe a parallel behaviour for the dry measurements.

The largest difference in Young's modulus between taped and glued is around 0,65 GPa (14,2 GPa -13,55 GPa), this makes up for an error of 4,8% (assume glued is the 'true' value). The curves behave similarly for both Poisson's ratio and Young's modulus, except for hydrostatic measurement. It is uncertain why the comparison of the undrained hydrostatic measurements for both Young's modulus and Poisson's ratio behaves differently, it could be an artefact.

These observations can be summarized:

- The comparison shows small difference in the experimental values for both Young's modulus and Poisson's ratio, and the plots indicates a strong parallel behaviour between them;

- The core sample was put in the oven at higher temperature after first test. Draining the sample can create cracks, which makes the rock softer;
- Taped had a higher value for Young's modulus than glued in most cases. The effect is within an error, but perhaps this is due some small slippage between coupling;
- The higher value for Young's modulus for taped was also seen for the dry measurements. It is less likely to see any effect between gauges and core sample in this scenario. This observation indicates that it has nothing to do with slippage;
- The epoxy layer covering the surface of the core sample can perhaps change properties due to stress alteration and reheating, and it is uncertain how much the layer can actually affect the measurements.

5.1.2 Observations of Young's modulus on Castlegate sandstone

Figure 5.3 is valuable for looking into the sensitivity of the low frequency measurement. First saturated measurement was done under drained conditions. This was because the valve closing the pore fluid line was open, and the measurement had to be repeated after the hydrostatic test so it was possible to compare at the same pore pressure.

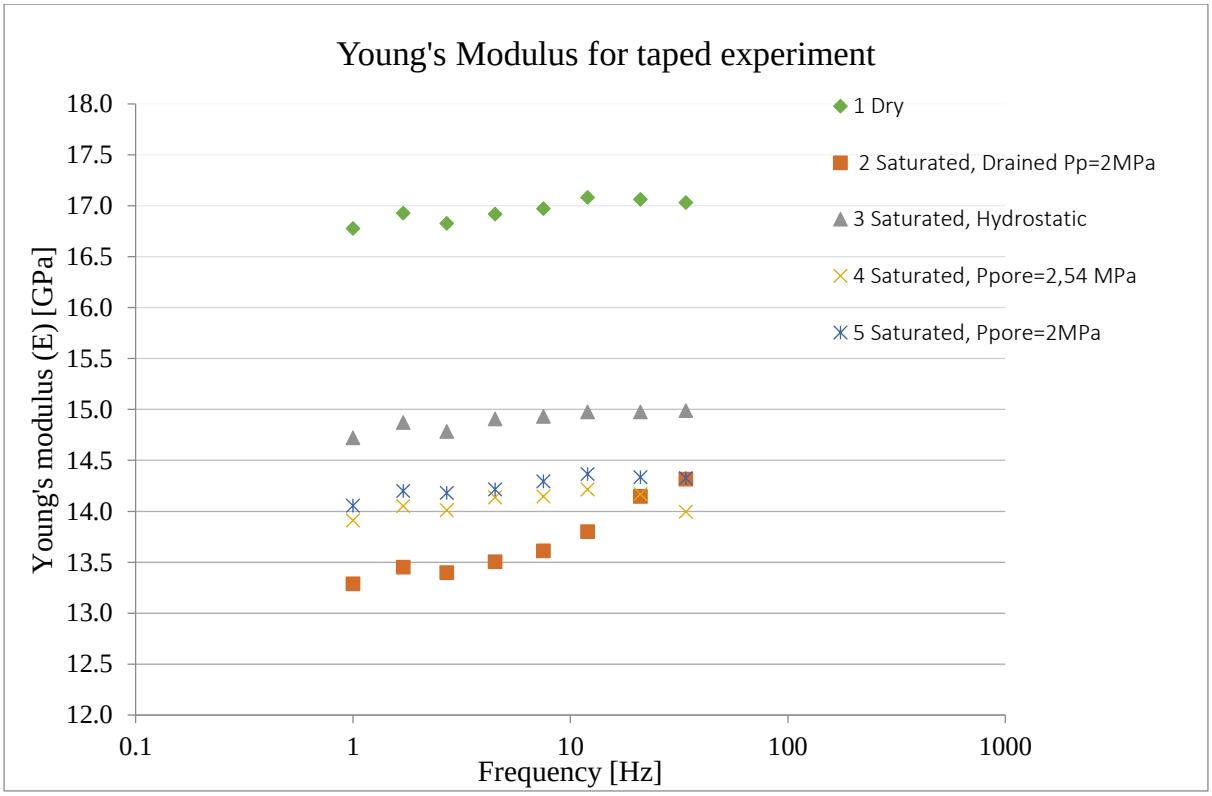

Figure 5.3 Young's modulus for taped experiment.

Stiffness

In Figure 5.3 one can see a clear difference in the Young's modulus from the dry measurement compared to the saturated. When the core sample is saturated it becomes softer, this is because the grains gets lubricated and it requires less stress to deform the sandstone. Remember equation(3.2), the strain is less for dry measurement under the same stress.

$$E = \frac{\sigma_x}{\varepsilon_x}$$

Measurement number 4 and 5 was taken under the same stress, but at slightly different pore pressure. Increasing the pore pressure results in a lower in Young's modulus. This can be explained by the effective stress, $\sigma' = \sigma - p_f$.

Measurement 4: $\sigma' = \sigma - 2,54MPa$

Measurement 5: $\sigma' = \sigma - 2MPa$

Attenuation - Drainage effect

Measurement number 2 in Figure 5.3 was performed under drained conditions, i.e. the valve is not closed, so the pore fluid can flow out form the core sample. At lower frequencies the sandstone is clearly softer, but at higher frequencies the Young's modulus is equal to the undrained measurement. This behaviour is due to the *drainage effect*. At lower frequencies the pore fluid has time to flow through the porous media, but at higher frequencies the deformation oscillates too quick for the pore fluid to flow back and forth (Fjær et al., 2008, p. 49):

$$C_D = \frac{k}{\eta_f}\frac{K_f}{\phi} \tag{5.1}$$

$$l_D^2 = C_D \tau_D \tag{5.2}$$

where k is the permeability, K_f is bulk modulus of pore fluid, and η_f is the viscosity of pore fluid. C_D is a measure of the length (l_D) the pore fluid can propagate during a given time τ_D. By using equation (5.1) and borrowing some rock properties from an earlier experiment on Castlegate sandstone *(Fjær et al., 2013)*, one can calculate a value for C_D. This is an estimate and more for curiosity and fun.

Table 5.1 Rock properties for Castlegate sandstone

Earlier measurements on Casltegate sandstone			
k	Φ	η_f	K_f
[mD]	[ ]	[Cp]	[GPa]
650	28,5	1	2,15

This gives a value for C_D ~0,09 m^2/s. Half of the length of the core sample is l_D = 0,00256 m. Then solving equation (5.2) for τ_D ~0,0135 s, results in a frequency of 73,8 Hz. From the figure it looks like the drainage effect disappears in the region of 60 Hz. The estimate was most likely lucky, however a close estimate compared to the measured response.

Dispersion effect

One can see a slightly increase in Young's modulus. This could be due to the dispersion effect. Amount of disperison differ from differently materials, and it is possible the dispersion is higher for increasing frequency. Section 2.1.2 explained the attenuation and phase shift. There was an attempt to measure the phase shift, but technical problems with equipment made the measurement useless. Reliable data for interpretation of the dispersion effect is hard to obtain, and the amount of measured data in the littature is limited (Fjær et al., 2008, p. 185).

For the first eight points, the largest difference in the Young's modulus is 4 %, except for the drained measurement. At the two highest frequencies the Young's modulus suddenly increases by quite a bit. This could be due to a various of reasons: resonance effects in equipment, gas (air) in the pore line and/or larger gas patches due to gas accumulation, ground noise from D/C power supply, dispersion effect, tilts etc. However, this increase is believed to be artefacts and will be ignored.

5.2 Measurement of non-elastic compliance

5.2.1 Low frequency measurements of first and second harmonic

The results from the second harmonic on Castlegate are clearly an artefact. It was decided to present one plot of the results anyway, since much time has been spent obtaining and understanding the nonlinear elastic effect. Also, even though the measurements were not as expected, a more detailed investigation of the results might discover something for the dependence of stress for the rock stiffness. It is presented in Figure 5.4 together with the measurements on PEEK. Since PEEK is a linear elastic material, the second harmonic should be close to zero, but the strain is even higher. A short summary will be presented after the plot, and the tables for the measured values are attached in Appendix B.

The non-elastic compliance for the dynamic measurement is presented in Figure 5.5, and the plot for the static measurement for the non-elastic compliance is presented in Figure 5.6. Since the static measurement obtain the strain for the LVDT's, a correction for aluminium

had to be done. This is because the LVDT's also measure some of the deformation from the endcaps. The extra deformation is subtracted and the blue plot (round marker) in Figure 5.6 is the corrected non-elastic compliance.

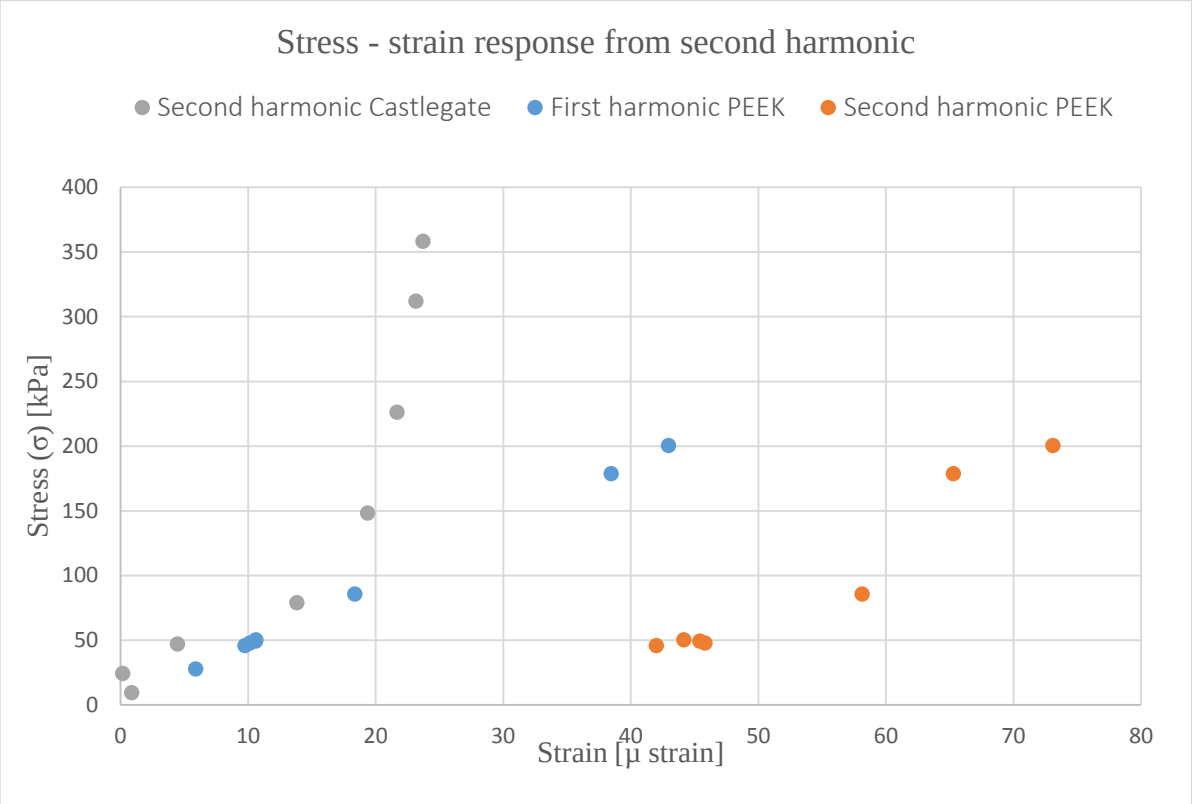

Figure 5.4 Stress strain plot of first and second harmonic. The blue dotted line represents the trend line for the first harmonic. Remember PEEK is more soft than Castlegate.

From Figure 5.4 you can see the stress - strain plot for the second harmonic on Castlegate and PEEK. There are reasons to believe resonance in the sample interfered with the signals, but even at low frequencies (0,1 Hz & 0,5 Hz) the measurements on PEEK show high values for the second harmonic. It is most likely resonance in the equipment itself. If this problem can be sorted out, it will be possible to investigate the contribution of the second harmonic in the future.

Table 5.2 Stress and strain values for plotting the non-elastic compliance in Figure 5.5

Stress ($\Delta\sigma_{RMS}$)	√2·Stress ($\Delta\sigma_{RMS}$)	Strain ($\Delta\varepsilon_{RMS}$)	Strain ($\Delta\varepsilon_{RMS}$) / Stress ($\Delta\sigma_{RMS}$)
[MPa]	[MPa]	[μ strain]	[GPa^{-1}]
0,009	0,013	0,654	0,0704
0,024	0,034	1,704	0,0702
0,047	0,066	3,284	0,0701
0,079	0,112	5,570	0,0706
0,148	0,209	10,645	0,0719
0,226	0,320	16,569	0,0733
0,312	0,441	23,394	0,0750
0,358	0,507	27,026	0,0754

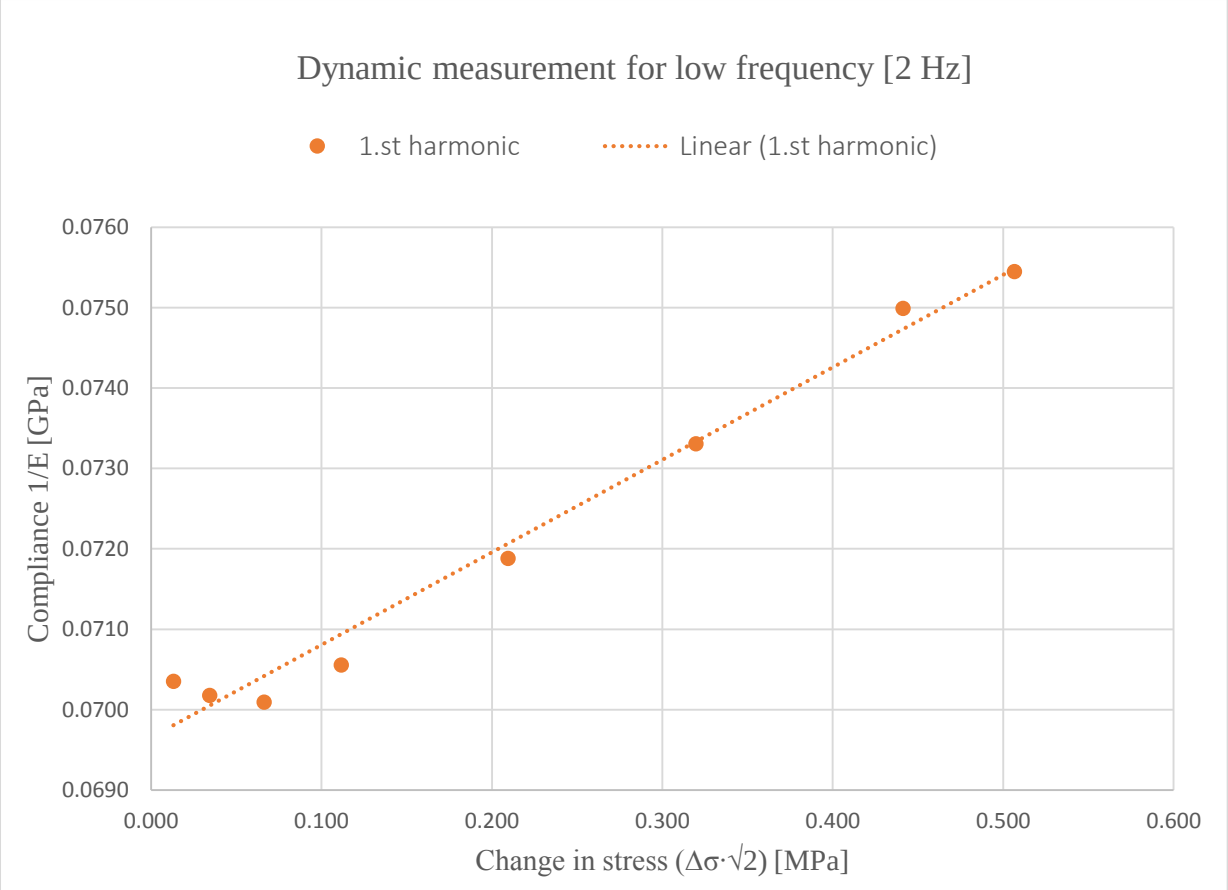

Figure 5.5 Non-elastic compliance versus change in stress for dynamic measurement.

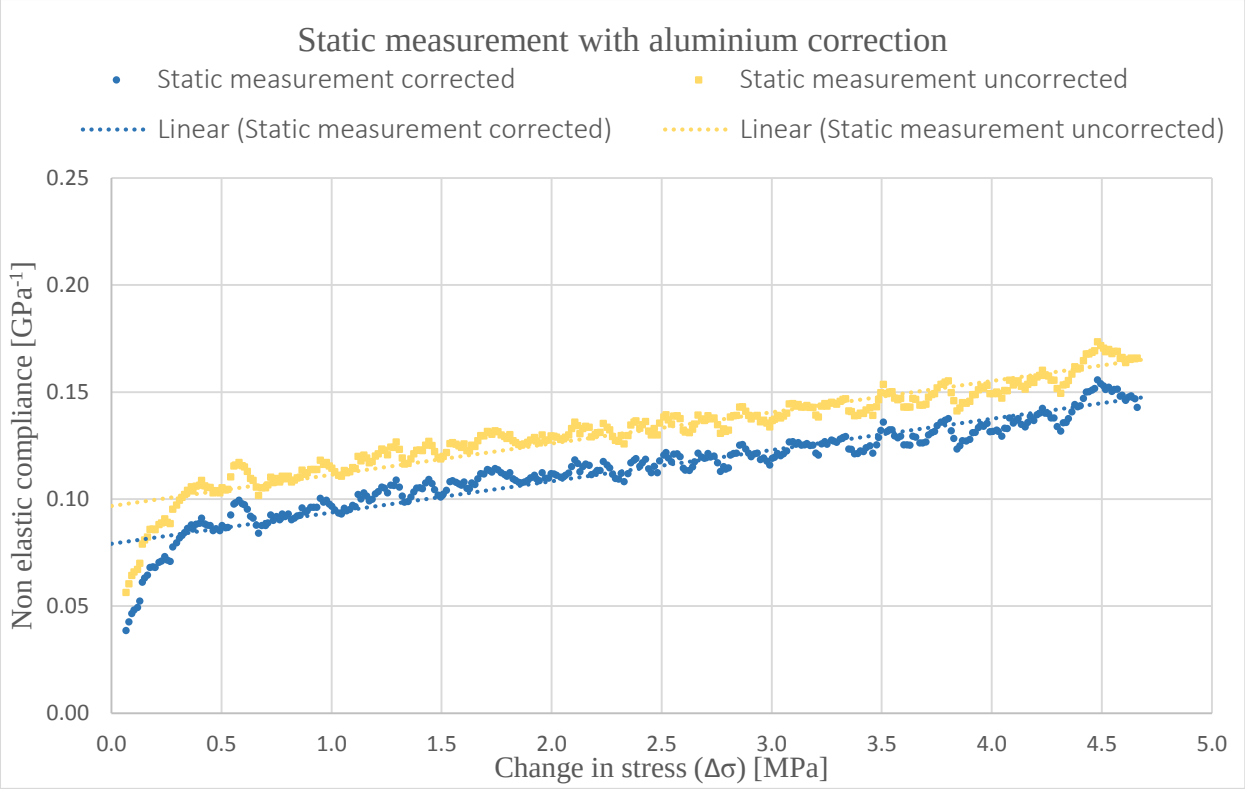

Figure 5.6 Correction of static measurement. Yellow plot is without the aluminium correction. Blue plot is corrected.

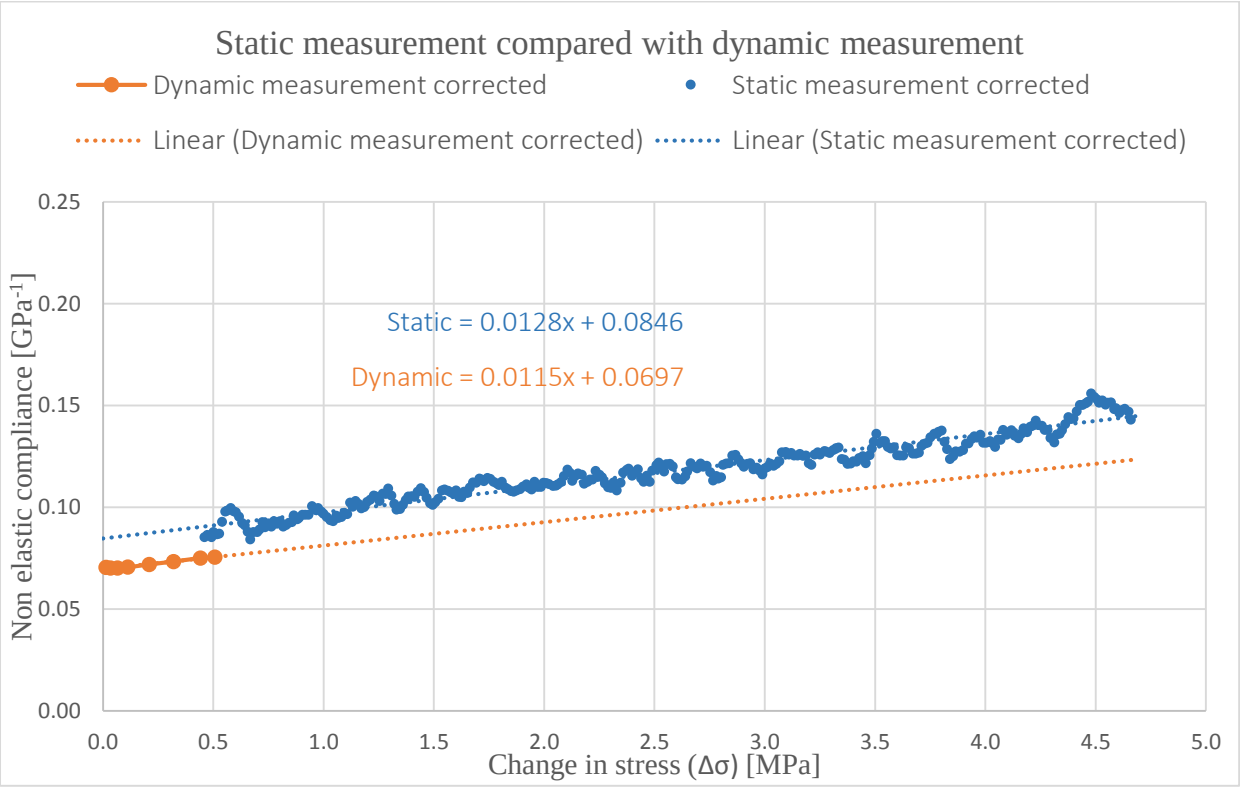

Figure 5.7 Comparison of dynamic and static measurement.

Dynamic measurement

The data points in Figure 5.5 are plotted as the non-elastic compliance (invers of Young's modulus) versus the change in stress, and the linear trend line is the function from equation (3.14). Notice that the first data point is a bit off from the linear trend line. In Table 5.2 on can see that the stress is very low due to the low force voltage amplitude in the beginning of the measurement. The lock-in amplifier was struggling getting a stable measurement because of the low signal, and it could be more noise instead of a correct value.

Static measurement

Figure 5.6 present the plot for the static measurement of the deformation versus the change in stress (unloading from 19 MPa to 14 MPa). As mentioned in the beginning of the section, a correction for the measured deformation by the LVDT's was needed. Since mechanical properties of aluminium are well-known, one can calculate the theoretical deformation for different stress alternation. Then by performing a static measurement using an aluminium core, the measured deformation can be subtracted by the theoretical. Then the difference left, will be the deformation from the endcaps. The measured static deformation on Castlegate needs to be subtracted by the deformation from the endcaps. The correction is presented in Figure 5.6. This made a difference of the non-elastic compliance of approximately 0,018 GPa^{-1}, which results in a decrease of the non-elastic compliance of about 16%.

The plot has included the non-elastic compliance in the measured range of 0 to 0,5 MPa. It was stated in section 3.2.1 that a minimum length is required to establish a true gradient value for the static measurement (avoid artefacts). Therefore, these values are not representative and will be excluded when comparing with the dynamic measurements.

Comparing static and dynamic

The static measurement and dynamic measurement is presented together in Figure 5.7. The trend line for both measurements are included, and the linear equations are presented as well. By using these equations, one can calculate the difference in the non-elastic compliance. Values are given in Table 5.3 below.

Table 5.3 Values obtained from the trend line for the dynamic and static measurement.

Stress (Δσ)	*Static*	*Dynamic*	*Difference*	*Percentage difference*
[MPa]	[GPa^{-1}]	[GPa^{-1}]	[GPa^{-1}]	[%]
0	0,085	0,070	0,015	17,612
2,5	0,117	0,098	0,018	15,651
5	0,149	0,127	0,022	14,536

5.2.2 Summary of observations and discussion

The difference is approximately 15% between the static and dynamic non-elastic compliance. Below are some considerations and thoughts to why they do not fully overlap.

- Static and dynamic measurements were done by using completely different sensors for both stress and strain, this can be an explanation for this difference;
- The static measurement is believed to be accurate, but some tilting was noticed for the LVDT's for the experiment for taped versus glued strain gauges. This was fixed, but it could still affect the measurement to some small extent;
- Higher harmonics have a possible effect on non-elastic compliance. This is not investigated in this thesis, but it is believed the effect is within the negligible;
- The assumption that the Young's modulus exhibits a similar relationship as the uniaxial compaction modulus could need some small correction.

The observations from last section can be summarized:

- The dynamic measurement of the non-elastic deformation appears to grow linearly with stress alteration;
- Application of the method (equation derived) for the dynamic non-elastic compliance has a similar trend line as the static. The variable in the linear equations deviate; within 10 %, and the values from the plots have a difference of approximately 15%.
- There are some small errors, but the overall measurements demonstrate good quality of the experimental data.

6 Conclusion and outlook

In order raise attention to the research of non-elastic rock properties, it is important to highlight its potential to bring new additional information on particular cracks and fractures for field applications. This thesis has looked into the non-elastic rock properties by utilizing direct dynamic measurements. It has investigated the empirical method describing the linear relationship between the non-elastic compliance and stress, through comparing dynamic measurements with static measurements. The purpose was to better understand the plasticity effects and quantify them.

- The dynamic measurement indicates that the linear relationship between the non-elastic compliance and stress is valid in the range close to the turning point;
- Strong correlation between trend line for dynamic and static non-elastic compliance.

The results from the dynamic measurement indicates that the static non-elastic compliance behaves linear in the extrapolated range, and strengthens the method behind combining static and dynamic measurements for evaluation of elastic dispersion.

Concerns from the scientific community lead to an investigation of taped versus glued strain gauges. This thesis has compared the Young's modulus and Poisson's ratio from two separate tests on the same Castlegate sandstone sample.

- Highest difference between Young's modulus measurement was 5 percent, and the plots indicates a strong correlation between taped and glued experiment;
- The dry measurements had the same difference and parallel behaviour as the saturated. This strengthens the reliability for the saturated measurements.

The results do not give an identification that taped gauges result in different readings than glued gauges. However, a direct proof is difficult since the rock sample stiffness might change between experiments.

6.1 Outlook

One of the focuses of this thesis was the investigation of the plasticity effect. The method of combining static and dynamic measurement for evaluation of non-elastic rock properties is new and still being researched.

Investigate gap

The direct dynamic measurements and the measurements from the LVDT's had a small difference in value. It is unknown if this difference is real or due to experimental errors. The following points should be looked at in future studies.

- Any dispersion effect for dynamic measurements at 2 Hz;
- Check and verify if the static unloading is to be compared to 1-2 Hz;
- Perform low frequency dynamic measurements on shale to compare.

Comparable experiments on Castlegate

Further investigation on Castlegate should include:

- Measurement of attenuation as difference between signal phases from strain gauges attached on the sample and aluminium standard;
- Direct recording of the hysteresis loop for large-amplitude stress modulations.

Higher harmonics

Second harmonic might give additional information on particular cracks and fractures in field applications. Further work should continue investigate the stress dependence of the rock stiffness.

- Investigate the second harmonic that comes from the measuring devices, and develop a method to compensate for it to be able to detect stress-strain response of sample itself on higher harmonics;
- Investigate the nature of higher harmonic responses and their cause (cracks and fractures).

Taped and glued strain gauges

To improve the certainty of the method of taping strain gauges, further work should investigate:

- Repeat experiment, but have one pair taped and the other glued;
- Perform glued before taped, and then compare with the data from this thesis.

7 Bibliography

Batzle, M. L. H., De-Hua, & Hofmann, R. (2006). Fluid mobility and frequency-dependent seismic velocity - Direct measurements.

Chenevert, M. A. (1997). *Shale preservation and testing techniques for borehole stability studies*. Paper presented at the IADC Drilling Conference, Amsterdam, Neth, 4-6 March.

Connell, S. (2004). Symmetric / antisymmetric wave functions. from School of Physics, University of the Witwatersrand.

Cregger, D. M., & Lamb, T. J. (1984). *Poisson's Ratio As A Parameter For Determining Dynamic Elastic Modulus*.

E. Kozlov, N. B., V. Motruk, A. Rusalin, L. Persidskaya, O. Kirseleva and A. Bovykin (2009). Integrating seismic attributes to estimate transport properties of dual porosity reservoir rocks. *First Break*(Vol 27, No 5, May 2009 pp. 43 - 52), 10. doi: 10.3997/1365-2397.2009008

Fahy, F. (2001). *Foundations of engineering acoustics*. San Diego, Calif: Academic Press.

Fjær, E., Holt, R. M., Horsrud, P., Raaen, A. M., & Risnes, R. (2008). *Petroleum related rock mechanics* (2nd ed. ed. Vol. 53). Amsterdam: Elsevier.

Fjaer, E., Holt, R. M., Nes, O. M., & Stenebraten, J. F. (2011). *The Transition From Elastic to Non-elastic Behavior*.

Fjaer, E., Holt, R. M., & Stroisz, A. M. (2012). *Combining Static And Dynamic Measurements For Evaluation of Elastic Dispersion*.

Fjær, E., Stroisz, A. M., & Holt, R. M. (2013). Elastic Dispersion Derived from a Combination of Static and Dynamic Measurements. *Rock Mechanics and Rock Engineering, 46*(3), 611-618.

Hoffman, R. (2011). *Frequency dependent elastic and anelastic properties of clastic rocks.* (PhD), Colorado school of Mines

Kramer, L. Y., Hugh D. (2012). *University physics, 13th edition, Young and Freedman*. San Francisco: CA : Pearson

Rossmanith, H. P. (1978). *The Role of Rayleigh Waves In Rock Mechanics,*.

8 Nomenclature

8.1 Abbreviations

cP	-	Centipoise
Hz	-	Herts
LVDT	-	Linear variable differential transformer
mD	-	Millidarcy
PEEK	-	Polyether ether ketone
P-wave	-	Primary / Pressure wave
S-wave	-	Secondary / Shear wave

8.2 Parameters

A	-	Cross-sectional area
C_D	-	Measure of the length (l_D) pore fluid can propagate during given time (τ_D)
E	-	Young's modulus (Rock mechanics)
E	-	Electric field (Electricity)
$E_{\tan}$	-	Tangent value of Young's modulus
E_e	-	Dynamic, elastic Young's modulus from P-wave velocity
f	-	Frequency
F	-	Force
G	-	Shear modulus
GF	-	Gauge factor
H	-	Static uniaxial compaction modulus

H_e - Dynamic (ultrasonic) uniaxial compaction modulus

I - Current

J - Current density

k - Permeability

K - Bulk modulus

K_f - Bulk modulus pore fluid

p_f - Pore pressure (fluid)

q - Charge

Q - Quality factor for attenuation

R - Resistance

S_H - Non-elastic compliance

T - Period (duration of one repeating cycle)

u - Amplitude reduction

u_0 - Amplitude initial size

v - Velocity wave

v_d - Drift velocity (Electricity)

V - Voltage

V_p - P-wave velocity

Greek alphabet

α - Measure of attenuation (Acoustics)

α - Poisson's ratio (Rock mechanics)

ε - Strain

φ	-	Porosity
η	-	Number of charges
θ	-	phase shift
ρ	-	Rock density
ρ_R	-	Resistivity of a material
σ	-	Stress
σ'	-	Effective stress
ω	-	angular velocity

9 Appendix

9.1 A

Ohm's Law:

$$V = I \times R$$

And from Weathstone bridge:

$$I_1 = \frac{V_{in}}{R_1 + R_4}$$
$$I_2 = \frac{V_{in}}{R_2 + R_3}$$
$$V_{AB} = I_1 \times R_1$$
$$V_{BC} = I_2 \times R_2$$

Then voltage out:

$$V_{out} = V_{AB} - V_{BC} = \frac{V_{in}}{R_1 + R_4} R_1 - \frac{V_{in}}{R_2 + R_3} R_2$$

Since one can set opposite resistance equal to each other:

$$R_1 = R_3 = R + \Delta R$$
$$R_2 = R_2 = R$$

Then we can redefine V_{out}:

$$V_{out} = \frac{R + \Delta R}{R + \Delta R + R} - \frac{R}{2R + \Delta R} = \frac{\Delta R}{2R + \Delta R}$$

$$V_{out} = \frac{\frac{\Delta R}{R}}{2 + \frac{\Delta R}{R}}$$

This latest expression for V_{out} is the same as in equation (4.6). The expression for strain can be found by using the relationship:

$$\frac{\Delta R}{R} = \varepsilon \times GF$$

Then equation (4.6) can be expressed differently:

$$V_{out} = \frac{\frac{\Delta R}{R}}{2 + \frac{\Delta R}{R}} = \frac{\varepsilon \times GF}{2 + \varepsilon \times GF}$$

Solving this equation for the strain ε gives

$$\varepsilon = \frac{2V_{out}}{GF \times V_{in} - GF \times V_{out}} = \frac{2V_{out}}{GF \times V_{in}} \quad \text{since } V_{in} \gg V_{out}$$

Which is the equation (4.7)

9.2 B

Table 9.1 Different values on Castlegate for the force voltage amplitude (V_{rms}). Values are presented in Figure 5.4.

Sine Input	Strain (ε_{RMS}) 1st	Strain (ε_{RMS}) 2nd	Stress (σ_{RMS})
[V_{rms}]	[u strain]	[u strain]	[k Pa]
0,1	0,65	0,88	9,3
0,3	1,70	0,17	24,3
0,5	3,28	4,46	46,9
1,0	5,57	13,81	78,9
2,0	10,65	19,37	148,1
3,0	16,57	21,68	226,0
4,0	23,39	23,17	312,0
4,5	27,03	23,71	358,2

Table 9.2 Different values and frequencies on PEEK for the force voltage amplitude (V_{rms}). Values are presented in Figure 5.4.

Sine Output	Frequency	Strain (ε_{RMS}) 1st	Strain (ε_{RMS}) 2nd	Stress (σ_{RMS})
[Vrms]	[Hz]	[u strain]	[u strain]	[k Pa]
1,0	0,1	5,89	66,86	27,7
1,0	0,5	10,14	45,81	47,7
1,0	1	10,58	45,41	49,2
1,0	2	10,60	44,16	50,1
4,0	2	42,96	73,11	200,4
1,0	105	9,76	42,00	45,7
2,0	105	18,35	58,15	85,6
4,0	105	38,47	65,29	178,5